THESIS

A SIMPLE PARAMETERIZATION OF AEROSOL EMISSION IN RAMS

Submitted by

Theodore Letcher

Department of Atmospheric Science

In partial fulfillments of the requirements

For the degree of Master of Science

Colorado State University

Fort Collins, Colorado

Spring 2013

Masters Committee:

Advisor: William Cotton

Sonia Kreidenweis
Jorge Ramirez

ABSTRACT

A SIMPLE PARAMETERIZATION OF AEROSOL EMISSIONS IN RAMS

Throughout the past decade, a high degree of attention has been focused on determining the microphysical impact of anthropogenically enhanced concentrations of Cloud Condensation Nuclei (CCN) on orographic snowfall in the mountains of the western United States. This area has garnered a lot of attention due to the implications this effect may have on local water resource distribution within the Region. Recent advances in computing power and the development of highly advanced microphysical schemes within numerical models have provided an estimation of the sensitivity that orographic snowfall has to changes in atmospheric CCN concentrations. However, what is still lacking is a coupling between these advanced microphysical schemes and a real-world representation of CCN sources. Previously, an attempt to representation the heterogeneous evolution of aerosol was made by coupling three-dimensional aerosol output from the WRF Chemistry model to the Colorado State University (CSU) Regional Atmospheric Modeling System (RAMS) (Ward et al. 2011). The biggest problem associated with this scheme was the computational expense. In fact, the computational expense associated with this scheme was so high, that it was prohibitive for simulations with fine enough resolution to accurately represent microphysical processes. To improve upon this method, a new parameterization for aerosol emission was developed in such a way that it was fully contained within RAMS.

Several assumptions went into generating a computationally efficient aerosol emissions parameterization in RAMS. The most notable assumption was the decision to neglect the chemical processes in formed in the formation of Secondary Aerosol (SA), and instead treat SA as primary aerosol via short-term WRF-CHEM simulations. While, SA makes up a substantial por-

tion of the total aerosol burden (much of which is made up of organic material), the representation of this process is highly complex and highly expensive within a numerical model. Furthermore, SA formation is greatly reduced during the winter months due to the lack of naturally produced organic VOC's. Because of these reasons, it was felt that neglecting SOA within the model was the best course of action.

The actual parameterization uses a prescribed source map to add aerosol to the model at two vertical levels that surround an arbitrary height decided by the user. To best represent the real-world, the WRF Chemistry model was run using the National Emissions Inventory (NEI2005) to represent anthropogenic emissions and the Model Emissions of Gases and Aerosols from Nature (MEGAN) to represent natural contributions to aerosol. WRF Chemistry was run for one hour, after which the aerosol output along with the hygroscopicity parameter (k) were saved into a data file that had the capacity to be interpolated to an arbitrary grid used in RAMS.

The comparison of this parameterization to observations collected at Mesa Verde National Park (MVNP) during the Inhibition of Snowfall from Pollution Aerosol (ISPA-III) field campaign yielded promising results. The model was able to simulate the variability in near surface aerosol concentration with reasonable accuracy, though with a general low bias. Furthermore, this model compared much better to the observations than did the WRF Chemistry model using a fraction of the computational expense.

This emissions scheme was able to show reasonable solutions regarding the aerosol concentrations and can therefore be used to provide an estimate of the seasonal impact of increased CCN on water resources in Western Colorado with relatively low computational expense.

ACKNOWLEDGMENTS

I would like to take this opportunity to acknowledge all of the people who made this thesis possible. I would like to start by first acknowledging my primary advisor, Dr. William Cotton, for providing his candid advice and valuable guidance. I would also like to thank the remainder of my thesis committee, Dr. Sonia Kreidenweis and Dr. Jorge Ramirez. Without your additional guidance, this thesis would have never come to fruition. I also wish to acknowledge the National Science Foundation for providing funding for this research through grants ATM 0835421 and AGS 1138896.

Outside of my committee I would like to thank Dr. Gustavo Carrio for helping me develop some of the code used within the emissions scheme. Similarly, I wish to acknowledge Steve Saleeby and Steve Herbener for helping to troubleshoot various coding errors and issues associated with the RAMS model. I would also like to acknowledge Dr. Dan Ward for all of his help initially in compiling and running WRF-CHEM. I also wish to extend my gratitude to Michal Clavner for discussing with me various data analysis techniques and for letting me use her computer to test the MPI capabilities of my code.

In addition to all of the people mentioned above, I would like to acknowledge anyone who has helped me move towards writing this thesis. This includes professors, administrators, computer technicians, friends, co-workers and family. Your support has proven invaluable throughout the past two and a half years.

TABLE OF CONTENTS

Chapter 1: Introduction

Aerosol cloud interactions are of potentially great importance to the large scale climate of the Earth (IPCC, 2007). Additional aerosols serving as Cloud Condensation Nuclei (CCN) (largely from anthropogenic activity) can alter the radiative properties of clouds, as well as their ability to produce precipitation (1st and 2nd aerosol indirect effects: Twomey, 1974 & Albrecht, 1989). On a more regional scale it has been suggested through observational evidence and numerical modeling that increases in CCN can modify the growth of precipitation within orographic clouds (Cotton and Levin, 2009). This has major implications for mountainous regions where much of the water supply is derived from seasonal orographic snowfall (Cotton and Levin, 2009). Of particular interest is the inter-mountain region of the western United States (specifically the Colorado Rockies) where, recently, a number of field campaigns and modeling experiments have contributed substantially to the literature surrounding the modification of orographic snowfall by pollution aerosol.

It is currently understood that increased CCN lead to smaller/more numerous cloud droplets within the supercooled cloud region of an orographic "seeder-feeder" (Fig.1.1, from Cotton et al., 2010) cloud system (Borys et al. 2000). Smaller cloud droplets within the supercooled "feeder" rime less efficiently onto pristine ice crystals that precipitate from the above "seeder."

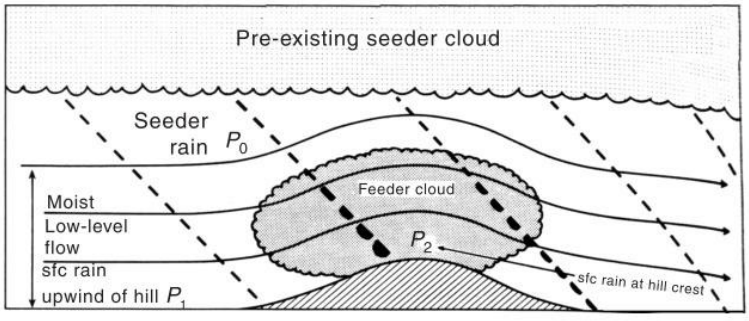

Figure 1.1: Feeder-seeder cloud system. From Cotton et al. 2010, adapted from Bergeron, 1965

This process has a two-fold effect on orographic snow. First, it effectively delays or inhibits the conversion of cloud water into precipitation, thus reducing the total amount of snowfall from the orographic storm. Second, the unrimed snowflakes are more easily advected downstream to the lee of the mountain barrier, causing an overall shift in precipitation that ultimately changes the distribution of water resources within these mountainous regions.

The goal of this research is to expand the knowledge surrounding this effect by introducing an emissions parameterization for CCN into the Regional Atmospheric Modeling System (RAMS) that is both consistent with the available observations and computationally efficient. This research will accomplish this goal by investigating the climatological aerosol observations in the US intermountain west to help justify the assumptions made in the emissions parameterization. The parameterization will then be compared to observations gathered at Mesa Verde National Park (MVNP) during the Inhibition of Snowfall by Pollution Aerosol (ISPA) III campaign. For the bulk of this research, the aerosol sources used in the RAMS emissions parameterization will be derived from Weather Research and Forecasting Chemistry (WRF-CHEM) model output. For additional validation, the parameterization will be compared to WRF-CHEM as well as the ISPA-III observations. As a final undertaking, this parameterization will then be used as part of an orographic snowfall case-study to better estimate the magnitude of the ISPA effect.

1.2: Background

1.2.1: Aerosol effects on Orographic Snow:

Evidence for the ISPA effect was first presented by Borys et al. (2000). This paper presented evidence (derived from observations collected at the Storm Peak Laboratory [SPL]

near Steamboat Springs, CO) of an indirect relationship between Clear Air Equivalent (CAE) sulfate concentrations and cloud droplet size during orographic snowstorms. A similar relationship was found for CAE sulfate and snowfall rate. Subsequently a direct relationship was observed between CAE sulfate and droplet concentration. The inference made by Borys et al. was that higher CAE sulfate was associated with higher concentrations of CCN, and caused a reduction in snowfall due to the inhibition of riming resultant from smaller droplets within the supercooled orographic cloud. Further support for this theory came from Borys et al. (2003), where they were able to visually confirm that snowflakes were indeed less rimed under high CAE sulfate conditions than they were under low CAE sulfate conditions.

Further observational evidence for snowfall reduction by anthropogenic pollution was presented in a study by Givati and Rosenfeld (2004). Their study compared 100 years of precipitation records downwind of pollution centers to precipitation downwind of areas they considered unaffected by pollution. They developed a ratio (R_0) to analyze these data in the context of orographic precipitation. They defined R_0 as the ratio of the precipitation on a mountain slope to precipitation in an upwind lowland region. By using this method they were able to find statistically significant decreases in R_0 (~20%) with time downwind of pollution centers, with no coinciding decrease downwind of areas unaffected by pollution. To draw their conclusions, they made the assumption that pollution increased with time in urban centers. From their results, they determined that the decreases in R_0 were associated with decreases of precipitation on windward mountain slopes. Since they suggested that pollution was increasing in time, they were able to attribute this decrease in R_0 to the ISPA effect. Additionally, they found evidence of an increase in snowfall (~14%) on lee mountain slopes. They suggested that unrimed snowflakes, because they are lighter than rimed snowflakes, are more easily advected

over the mountain barrier by the horizontal wind. This was termed the "spillover effect". Since Givati and Rosenfeld (2004), similar observational studies have drawn a link between decreases in upwind orographic precipitation and increase in anthropogenic pollution aerosol, e.g., Jirak and Cotton 2005, and Rosenfeld and Givati 2006.

1.2.2: Advances in Numerical Modeling

Recent advances in computing power have led to the implementation of advanced microphysical schemes within high resolution numerical models (Levin and Cotton 2009). Some of the more notable advancements are presented in work done by Saleeby and Cotton (2004). While this paper discussed several upgrades to the RAMS microphysics, the most significant contribution was the introduction of a bin-emulating bulk microphysical droplet activation scheme into RAMS

. This scheme works by using look-up-tables, constructed by using the Lagrangian parcel model described by Heymsfield and Sabin (1989), to predict the fraction of activated CCN given the model atmospheric conditions. This significantly improved upon the bulk parameterizations for cloud droplet activation without increasing the computational requirements. This research paved the way for advanced microphysical studies on complex cloud systems that were previously too computationally expensive to simulate using binned activation schemes.

The original look-up-tables from Saleeby and Cotton (2004) used temperature, vertical velocity, aerosol number concentration, and aerosol median diameter to predict an activated fraction. The chemical composition of the aerosol was fixed and assumed to be that of ammonium sulfate. More recently, the look-up-tables were modified by Ward et al. (2011) to include the hygroscopicity parameter κ (Petters and Kreidenweis, 2007) as an independent

variable. This opened the door for researching the effects of aerosol chemical composition on cloud microphysics, as well as size and number concentration.

In addition to look-up-tables for aerosol nucleation, the upgrades made by Saleeby and Cotton (2004) to the RAMS microphysics included the introduction of a 2nd cloud-droplet mode for large cloud-droplets that nucleate on Giant CCN (GCCN), and a two-moment prediction scheme for hydrometeors. The inclusion of a 2nd cloud-droplet class makes it possible for RAMS to realistically simulate the bimodal cloud-droplet distribution often seen in nature, and the two-moment scheme allows for a smoother transition between the different hydrometeor classes (Saleeby and Cotton, 2004). The activation of GCCN is treated somewhat different than the activation of CCN. While Saleeby and Cotton did run the parcel model using GCCN, it was found that nearly 100% of GCCN activate and grow past the size limits allowed by the model, so instead of using the look-up-tables to activate GCCN, it is assumed that all GCCN activate in an environment with a relative humidity of 100% or greater.

A further upgrade to the RAMS microphysical package was the inclusion of a binned riming scheme (Saleeby and Cotton, 2008a). The new approach to riming significantly improves upon the previous bulk parameterization by replacing the empirically derived collection efficiencies for riming with a binned interaction between cloud-water and ice particles. This scheme does not represent a true binned scheme, as the shape of the hydrometeor size distributions do not change. Instead, the hydrometeor size distributions are divided into smaller bins that interact together, shifting the size distributions of each hydrometeor species. Once these interactions have taken place, the bulk size distributions are recalculated to represent the changes in number concentration and median diameter. Despite the fact that the shape of the hydrometeor size distribution is fixed, the binned riming approach provides a much more

realistic representation of riming than does the empirically derived bulk parameterization. It was found through validation of this model against data collected at SPL that the binned approach was able to more accurately represent the riming process in orographic clouds than the bulk parameterization (Saleeby and Cotton, 2008a).

These upgrades to the microphysics within RAMS have allowed for a more realistic representation of complex cloud systems without overburdening computational expense. As a result, modeling studies using RAMS have been able to shed new light upon the complex microphysical processes and feedbacks present within orographic snow storms.

1.2.3: Modeling Research:

Several of the recent modeling studies performed at Colorado State University have used the advanced microphysics package in RAMS to simulate the sensitivity of orographic snow to CCN. These studies are of high importance as a significant portion of the water resources within the Colorado Rockies comes in the form of orographic snow (Borys and Weztel, 1997). One study by Saleeby et al. (2008) used RAMS to simulate two separate orographic snowfall events measured during the ISPA-II field campaign at SPL in February of 2007 (Feb 11-13, and 23-25). Their experiment repeated each simulation varying the CCN concentrations from a "clean" surface concentration of 100 cm^{-3} to "polluted" 1900 cm^{-3}. They found that in the polluted simulations, for both case-studies, there was a decrease in precipitation on the windward side of the mountain and a corresponding increase in precipitation on the leeward side. However, the amplitude of this change was found to be largely dependent on the dynamical and microphysical aspects of each storm (Saleeby et al., 2008). The February 11-13 storm was characterized as having a relatively high Liquid Water Content (LWC) and heavily rimed particles within the

cloud compared to the Feb 23-25 storm, which was drier in nature and consisted mostly of unrimed ice crystals, as seen in the observations taken during the ISPA-II field campaign (Saleeby et al., 2008). In the drier case, increased CCN had a lesser effect on the precipitation than it did in the moist case. The interpretation was that, in drier clouds supercooled cloud droplets are already too small to rime efficiently and making them smaller by adding more CCN does not substantially alter the precipitation particles. A subsequent study by Saleeby et al. (2008) investigated the cumulative impact ISPA had during several winter seasons for the Colorado western slope. The results of this study indicated that, while the magnitude of the ISPA effect is highly variable from one year to the next, the San Juan Mountains in southwest Colorado are the most affected by ISPA, showing a 3-5% decrease of water resources in upwind water basins. This was attributed to the fact that orographic snowstorms forming in southwest Colorado are climatologically higher in LWC than the snowstorms that affect the northern part of the state, and therefore more susceptible to increased CCN.

The studies by Saleeby et al., provide good evidence that the inhibition of riming by increased CCN is the main physical mechanism responsible for ISPA, however, there are other papers in the literature that indicate orographic clouds can have a much more complicated response to CCN. One study by Lynn et al. (2007) found that increased aerosol concentrations can actually increase the LWC available for accretion within the supercooled region of the orographic cloud by shutting off collision-coalescence at lower elevations within the cloud, thus allowing more cloud water to be transported to higher up the mountain where it can rime onto snow hydrometeors. This would suggest that increased aerosol could, in certain cases, actually increase the amount of orographic snowfall on windward slopes. This result was also found by Muhlbauer et al. (2010), who went on to suggest that the sensitivity of orographic snow to CCN

was highly variable on a case-to-case basis. However, given that wintertime orographic precipitation in Colorado is almost entirely derived from cold precipitation processes, the cloud response to increased CCN seen by Lynn et al. is less of a factor within this region. This effect is more likely pertinent in the Sierra Nevada Mountains of Southern California, where maritime air-masses, rich in moisture, can generate clouds at altitudes low enough for warm-rain processes to occur.

These different modeling studies have provided great insight into the physical responses that occur within orographic clouds under varying CCN concentrations. However, what these studies lack are realistic representations of aerosol emission sources. Instead, these studies simply test the sensitivity of different orographic cloud systems and atmospheric conditions to increased CCN by repeating the same model simulations with varying CCN concentrations.

Until recently, there have been very few attempts to use accurate source representations of pollution and model-resolved aerosol chemistry in conjunction with models containing advanced microphysical schemes. Ward et al. (2011) is one exception. In this paper, an attempt was made to couple the Weather Research and Forecasting (WRF) Chemistry (WRF-CHEM) model to RAMS. This approach combined the benefits of a chemistry resolving atmospheric model with the benefits of an advanced microphysical package. However, several problems arose using this method. First and foremost, the computational of performing (even short) simulations at the spatial resolutions required to accurately simulate cloud microphysics were prohibitively expensive for the available computer resources. Additionally, Ward et al. (2010) used only the aerosol output from WRF-CHEM (as opposed to both aerosol and meteorological output) to nudge the CCN in RAMS, this left room for the meteorological discrepancies between the two models to generate spurious aerosol concentrations. Lastly, the representation of

chemistry within the WRF-CHEM modules used as part of this research was incompatible with the WRF-CHEM cloud scavenging scheme. As a result there was no cloud scavenging of aerosols, therefore, in cases involving clouds and precipitation, WRF-CHEM tended to overestimate the aerosol concentrations (Ward et al. 2010).

Despite these caveats, Ward et al. was able to find some success in using this method. In one case they found that WRF was able to accurately represent the evolution of an aerosol plume measured during the ICE-L field experiment over the High Plains of Eastern Colorado. This case, however, was devoid of precipitation, which reduces any errors related to cloud and precipitation scavenging. Furthermore, the aerosol plume had a local origin (Denver), so the influence of remote anthropogenic pollution on the total aerosol burden is left relatively unknown in this case.

1.2.4: Aerosol formation and chemistry

One of the major difficulties in trying to create an aerosol source parameterization scheme that is both reasonably accurate and computationally efficient is the representation of Secondary Aerosol (SA) formation processes, specifically the organic contribution to SA (SOA). SA formation is the process by which organic and non-organic gases (having both anthropogenic and natural origins) in the atmosphere undergo chemical reactions that enable them to enter the solid phase by either; condensing onto existing aerosol or forming new aerosol particles. SA formation inextricably links anthropogenic and natural emissions, generating new aerosol at locations far removed from urban pollution centers, making it difficult to predict CCN concentrations without a representation of atmospheric chemistry (Andreae and Rosenfeld (2008). In fact, Andreae and Rosenfeld (2008) made the argument that *only* a full chemistry

resolving atmospheric model with accurate representations of both anthropogenic and natural gas/aerosol emissions as well as aerosol physics could yield robust results regarding predicted concentrations of cloud-active aerosol. In spite of this statement, I make the argument that, under certain circumstances, scientifically relevant results can be found using simple CCN source parameterizations without resolving (explicitly) SA formation. The following literature review will help in making this case, focusing most of the attention of the SOA component of SA.

It has been shown previously that SOA formation is responsible for between 10-40% of the total organic aerosol mass, with regionally higher percentages (Volkamer et al. 2006). Furthermore it has been suggested that ~90% of SOA formation is formed from precursor gases that are biogenic in origin (Kanakidou et al., 2005). These studies help illustrate the importance of SOA on the global scale. However, the importance of SOA on regional and seasonal scales is much more variable. This variability is well illustrated by Liao et al. (2007). Liao et al. used the GEOS-CHEM model to express the importance of SOA to the total organic aerosol mass burden as the ratio between SOA and total Organic Aerosol (OA=SOA+POA). They found that during the winter (DJF) the ratio Secondary to OA (SOA/OA) of surface mass concentrations was small across the western United States, with values <0.1 for the Rocky Mountains of Colorado. Furthermore, they looked at the zonally-averaged SOA/OA ratio and found, that at the mid-latitudes, SOA/OA ratios did not reach values >0.1 until roughly 3km AGL during DJF. At this altitude CCN concentrations are low and will not likely have a measurable effect on orographic snowfall as this height is above the portion of cloud where riming takes place. Liao et al. found vastly different results for the summer months (JJA) where SOA mass accounted for nearly half of the total organic aerosol throughout much of the United States with regionally higher

amounts. This study suggests that during the wintertime, contributions of SOA to aerosol mass are somewhat limited. Similarly, Schichtel et al. (2008) reported significantly reduced carbonaceous aerosol concentrations during the winter (compared to summer) at pristine locations, e.g., Rocky Mountain National Park.

These studies are encouraging as they found that contributions of SOA to the total aerosol mass burden are small compared to primary aerosol emissions during the winter months. However they do not provide any information regarding seasonal changes in aerosol number concentration.

Further justification for neglecting secondary aerosol during the winter is explained by making a distinction between aerosol mass, and CCN concentration. As explained by Andreae and Rosenfeld (2008), increases in aerosol mass due to SA formation do not necessarily translate into changes in CCN concentration. As stated previously, organic gases can be converted into aerosol either by condensing onto existing particles, or by reacting with other gases to form new ones. Andreae and Rosenfeld (2008) explain that increases in aerosol concentration due to the formation of new particles likely do not immediately lead to local increases in CCN because the newly nucleated particles are far too small to be cloud-active. They go on to state that additions to aerosol mass by condensation do not necessarily increase CCN concentrations because condensation often occurs on aerosols already capable of serving as CCN.

Given that the observational evidence related to aerosol chemistry show a marked decline in the contribution from SOA mass during the winter months, it is hypothesized that a model can reasonably simulate the emission and transport of CCN by assuming that SA and SOA can be approximated as primary aerosol. Furthermore, the benefits of using a simple parameterization to source aerosol into the model in lieu of a full atmospheric chemistry model greatly outweigh

the limitations. The data analysis presented in the next chapter will provide further support for this statement by using climatological averages of aerosol chemistry and concentration along the Colorado western slope to reinforce the conclusions discussed in this chapter. Additionally, data from the Interagency Monitoring of Protected Visual Environments (IMPROVE) network will be used to reasonably quantify wintertime contribution of organic aerosol to the total aerosol burden.

Chapter 2: Climatological Aerosol Observations in Western Colorado

2.1: IMPROVE Climatological Data

Climatologically, the aerosol in the inter-mountain west of the United States is best described as "remote continental" (Ward et al. 2010). Remote continental aerosol is made up of a bimodal distribution in aerosol concentration with one peak of on average 4000 (cm^{-3}) within the Aiken size category (~20 nm), with a secondary peak of on ~3000 (cm^{-3}) centered over the accumulation mode sizes (100 nm) (Seinfeld and Pandis 2006). The chemical composition of remote continental aerosol is made up mostly of sulfate and organic carbon (Levin and Cotton 2009). It is thought that the sulfate portion of aerosol is derived mostly from anthropogenic sources, while most of the carbon is natural in origin. Aerosol data from the IMPROVE network was analyzed at four sites along the Colorado western slope to gain a better understanding of seasonal trends in background aerosol composition and to better quantify the contribution of organic aerosol to the total aerosol burden.

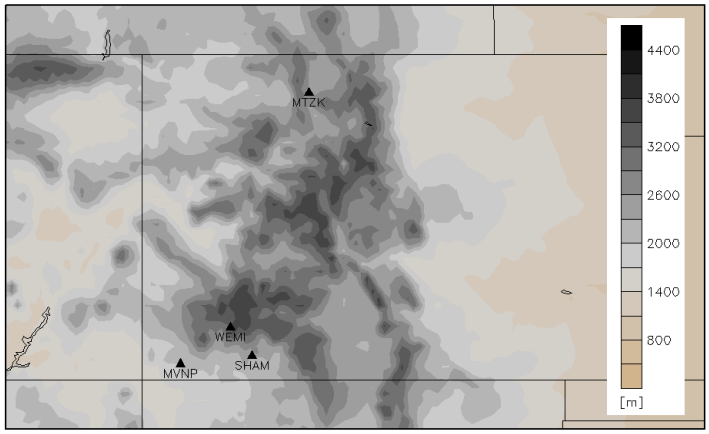

Figure 2.1: IMPROVE aerosol sites on the Colorado Western Slope

IMPROVE provides PM2.5 (Particulate Matter less than 2.5 μm in diameter) aerosol data at several protected sites throughout the United States. IMPROVE measures aerosol by allowing a filter to collect aerosol for one 24 hour period every three days. Chemical analysis of the filter provides information regarding the aerosol composition. The four IMPROVE sites chosen for this analysis were MVNP, Mt. Zirkel (MTZK), the Weminuche Wilderness (WEMI), and Shamrock Mine (SHAM),

the locations of these sites are shown in Fig. 2.1.

The chemical species included in the analysis were; ammonium sulfate, ammonium nitrate, sulfate, nitrate, elemental carbon, organic carbon and soil. Sea salt was not included because these locations are all well inland where sea salt is not a major contributor to aerosol mass (Ward et al. 2010). Fig. 2.2 shows the monthly averaged mass concentrations (μg m^{-3}) of each chemical species for the four chosen sites.

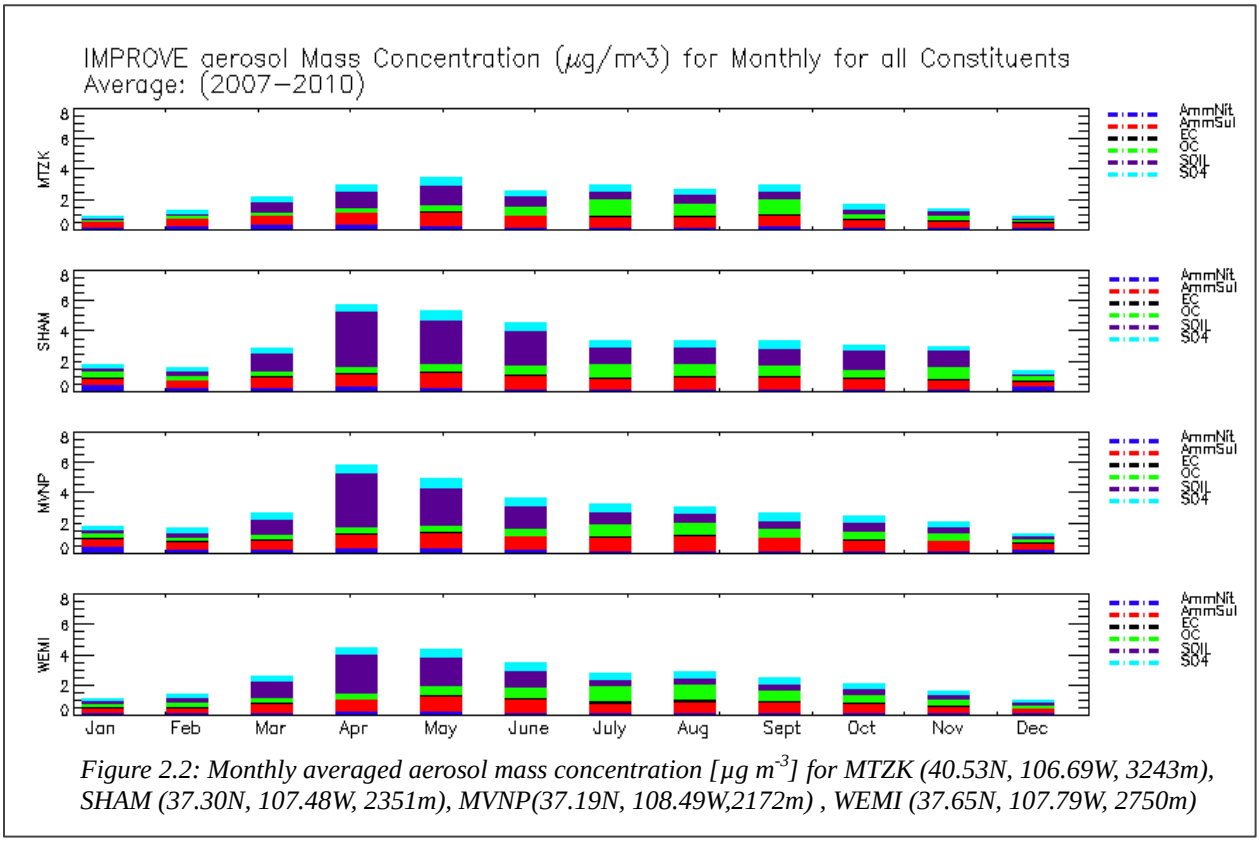

Figure 2.2: Monthly averaged aerosol mass concentration [μg m^{-3}] for MTZK (40.53N, 106.69W, 3243m), SHAM (37.30N, 107.48W, 2351m), MVNP(37.19N, 108.49W,2172m) , WEMI (37.65N, 107.79W, 2750m)

There is a highly visible seasonal cycle in both organic and soil mass, with soil becoming the dominant chemical constituent during the spring (MAM). Organic aerosol mass has a peak during the summer (JJA). Mt. Zirkel has a slightly less pronounced peak in soil fraction during the spring, perhaps due to its more northern location, and higher elevation, making it less prone to dust from the southwest U.S. compared to the other three sites. Sulfate mass shows much lower seasonal variability, although sulfate concentrations are generally higher during the

summer months, corresponding to a seasonal increase in photochemical activity. Mt. Zirkel has much lower observed aerosol mass concentrations compared to the other three sites, especially during the winter. This is likely due to the high elevation of the observation site, where there is less influence of boundary layer pollutants (Cozic et al. 2008).

Table 2.1 shows the annual average PM2.5 mass concentration for each chemical species at the four sites. In all locations, soil mass has the highest average mass concentration of the included chemical constituents, though this is a seasonal feature with the bulk of soil mass measured during the spring months. At all sites, concentrations of ammonium sulfate are higher than ammonium nitrate concentrations. Elemental (light absorbing) carbon contributes very little to the total aerosol mass, further indication that most of the carbon is likely biogenic in nature. Organic carbon has mass concentrations comparable to the sulfate and ammonium sulfate mass concentrations, fitting the description of remote continental aerosol given by Levin and Cotton (2009). These results show that for remote continental aerosol, natural sources of aerosol (assumed to constitute the organic fraction) are nearly as important to the total aerosol mass burden as anthropogenic sources (ammonium sulfate and nitrate). However, it cannot be determined from the IMPROVE network what percent of the observed organic carbon is made up of secondary aerosol, so the contribution of SOA to the aerosol mass is still undetermined.

*Table 2.1: Aerosol mass concentration [μg m^{-3}] average for each chemical species as measured by IMPROVE *Calculated from the measured SO_4^{2-} and NO_3^- mass.*

IMPROVE SITE	MVNP	WEMI	SHAM	MTZK	Average
Elevation [m]	*2172*	*2750*	*2351*	*3243*	----
$(NH_4)_2SO_4$*	0.73	0.6	0.68	0.6	0.65
$(NH_4)NO_3$*	0.19	0.11	0.18	0.16	0.16
Organic Carbon	0.48	0.51	0.54	0.45	0.5
Elemental Carbon	0.07	0.09	0.08	0.06	0.08
Soil	1.01	0.76	1.34	0.52	0.91
All	2.48	2.08	2.83	1.79	2.29

The large increases in soil aerosol during the spring associated with dust likely have a significant effect on orographic precipitation, as orographic storms during the spring months likely contain higher liquid water contents. Furthermore, dust aerosol can affect GCCN and IN, in addition to CCN concentrations, further complicating the microphysical response in orographic clouds. Lastly, the contribution of soil dust to near surface CCN concentrations is unknown as the ISPA campaigns have all occurred during time periods outside of the spring, so the observations available do not show the spring peak in dust mass. Given the climatology of chemical partitioning of aerosol in this region, an estimate of hygroscopicity can be made.

The hygroscopicity parameter (κ) was calculated from the IMPROVE network using equation 6 from Petters and Kreidenweis (2007), which assumes an internally mixed aerosol (this is usually a reasonable assumption [Andreae and Rosenfeld (2007)]). This simplifies the computation of κ to a volume-weighted average of each chemical species. The density and κ values for each chemical species were taken from Table 2 from Ward et al. (2011). The κ values

for all listed organic chemicals from Ward et al. were used to make an average calculated κ for the IMPROVE Organic Carbon (OC). With knowledge of mass, density, and κ for each chemical constituent, an overall κ is easy to calculate. The monthly averaged κ at each site is shown in Fig.2.3. κ has a seasonal cycle that is inverse to the seasonal cycle in mass concentration, with relatively high κ values during the winter, and lower κ values during the spring and summer months. This seasonal cycle in κ is qualitatively similar to the results from Levin et al. (2011). The lower κ values during the spring are almost certainly due to the very high soil (dust) fraction observed during this time.

From the low point during the spring, κ does not increase throughout the summer, despite a decrease in soil mass. This is because the aerosol organic fraction becomes higher at this time, and acts to reduce κ. During the late fall and early winter κ increases rapidly from

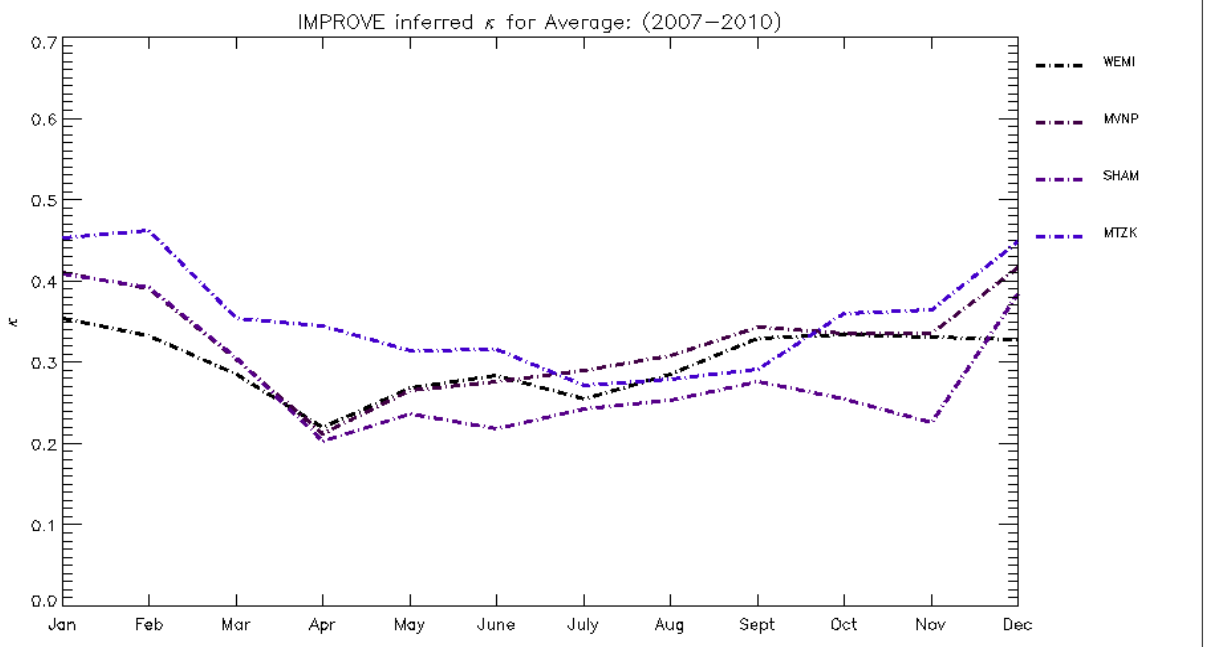

Figure 2.3: Annual cycle in κ calculated from IMPROVE

~0.3 to above 0.4. This increase is tied to a seasonal decrease in organic and soil mass

concentrations that allow for the hygroscopicity to be determined from more hydrophilic chemical species such as sulfate and ammonium sulfate. While the results here look qualitatively similar to Levin et al. (2011), Levin et al. recorded much lower values of κ in their observations. One reason is that dust is not typically found in particles smaller than 350nm, which they found to be the majority of CCN. A discussion of aerosol formation pathways and aging is also required to explain this discrepancy.

Aged organic aerosol that has had time to mix with anthropogenic aerosol can be relatively hygroscopic, despite a relatively large organic fraction (Levin and Cotton 2009). However, new organic aerosol that has not had time to mix with sulfates is more likely to have a lower κ. Because filter measurements provide no information about aerosol size, each of these situations can look similar in the measurements from IMPROVE. This makes determining an average hygroscopicity from IMPROVE tricky. This is particularly true for remote continental aerosol due to the large contribution from natural organic chemical species. The findings from Levin et al. (2011) help to illustrate the complexity of remote continental aerosol hygroscopicity. While overall they found that κ from the IMPROVE network was higher than their observations, they also found that κ was dependent on aerosol size, with lower κ values for smaller aerosols. They attributed this to a higher organic fraction at small aerosol sizes, indicating that the small particles observed at pristine locations are almost entirely organic in nature. This suggests that the small aerosols observed in remote continental regions are newly formed SOA that have not had the time to mix with anthropogenic pollution, whereas the larger particles have had the time to go through the aging process and therefore have a larger anthropogenic component. The results from Levin et al. help to fill in information regarding aerosol hygroscopicity missing from the IMPROVE network.

2.2: Mesa Verde Aerosol Data from ISPA III

The ISPA-III field project collected aerosol data at MVNP for nearly a month during the fall of 2009 (9/21-10/16). Aerosol data, including total number concentration (CN) and CCN at various super saturations were measured by two separate instruments, a Droplet Measurement Technologies (DMT) CCN-100, and a TSI3010 Condensation Particle Counter (CPC). These instruments were able to take observations of CN at 1s and 10s intervals respectively. The final data were recorded as a 30 minute running average. The average of CCN data includes only 15 minutes of data due to cycling through different super saturations (Ward et al. 2010). The total time-series for CN, CCN (SS=0.3%, SS=0.5%) and activated fraction (ss=0.3%) are shown in Fig. 2.4. This figure illustrates the high variability of the CCN concentration observed at MVNP. A more quantitative view of the observed variability at MVNP is seen in table 2.2. CCN3 and CCN5 are very highly correlated (r^2=0.94) and show a very weak positive (linear) relationship to CN ($r^2 > 0.05$). More interestingly a very strong negative relationship is seen between the activated fraction and CN. In this relationship, activated fraction is proportional (r^2=0.71) to one over the total number concentration. The high correlation between CN and activated fraction, and the low correlation between CN and CCN concentrations indicates that the number of CCN is more dependent on chemical or size changes in aerosol than it is on the number of aerosol available. However, this apparent high dependence of CCN activation is largely seen because these data include both Aiken and accumulation mode aerosol, without Aiken mode, it is likely that the CCN concentration would be more correlated with the total CN concentration. The presence of Aiken mode aerosol is punctuated by the occurrence of several High Particle Events (HPE) during the observation period. These are events in which the CN number concentration increases by double or more, with no corresponding increase in CCN.

These events are likely analogous to the Small Particle Events (SPEs) described by Levin et al (2011), and Boy et al, 2010, where it is suggested that the increases in aerosol concentration are due to rapid SOA formation.

Table 2.2: Mean, and standard deviation of the aerosol properties

Variable	Mean	STDEV
CN	1718.43	1438.60
CCN (ss=0.3%)	302.36	128.0
CCN (ss=0.5%)	479.5	204.35
Activated Fraction (ss=0.3%)	0.233	0.144

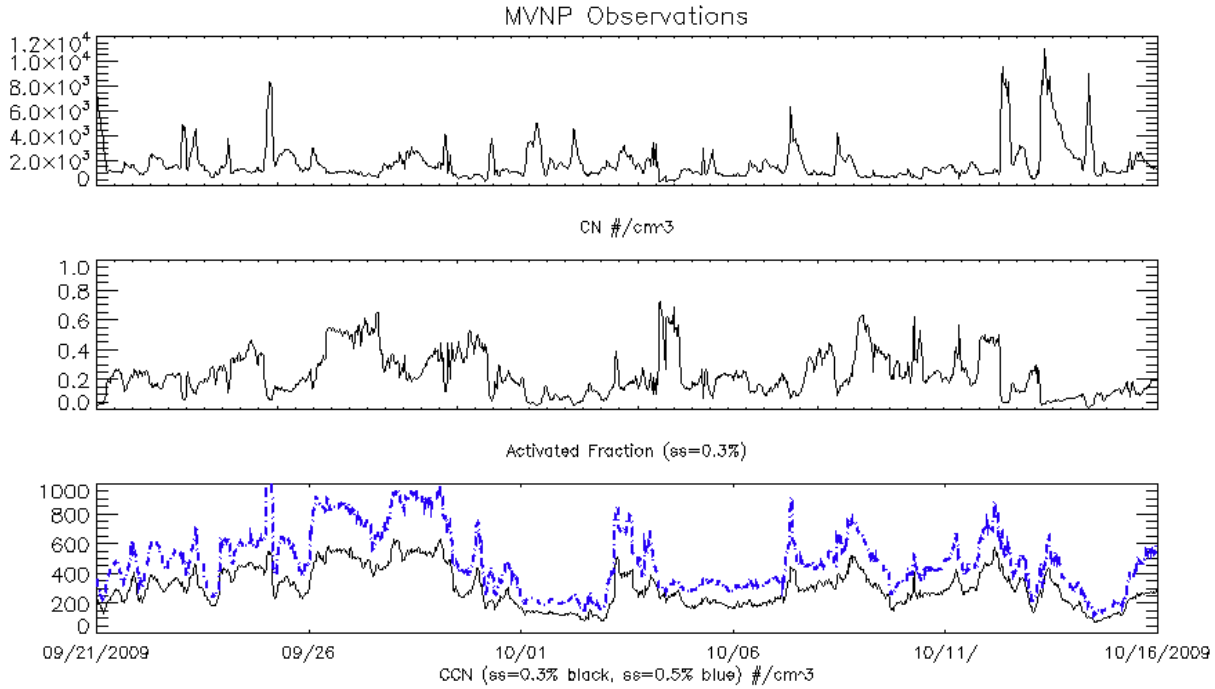

Figure 2.4: Time-series of CN (# cm^{-3}, Top), Activated Fraction (Middle) and CCN (# cm^{-3} Bottom) observed at MVNP during ISPA-III

Several HPEs were observed at MVNP during ISPA-III. These events were defined as rapid increases in CN concentration to at least two standard deviations above the mean CN

concentration, followed, subsequently, by a rapid decrease in CN back to near or below average levels. Four events were chosen for further analysis to investigate any similarities in the observed atmospheric conditions. Each event covered 48 hours both starting and ending at 00 UTC. The events chosen were: 09/25-09/27, 10/07-10/09, 10/12-10/14, and 10/14-10/16. Of the four events, only two were marked by a significant wind shift, with winds generally out of the east preceding the event shifting to out of the west during and after the event. The 10/12-10/14 case was accompanied by an increase in relative humidity and measurable precipitation, although this was not the case for any of the other HPEs. Working under the assumption that the HPEs observed at MVNP were associated with new particle formation, the fact that they occurred during a wide range of atmospheric conditions goes in support of some previous work that suggested that particle formation was dependent mostly on VOC and sulfate concentrations, and not meteorological conditions (Lewis et al. 1999, Boy et al, 2010).

The one coherent trend observed in all of the analyzed HPEs, was the presence of a recovery period for activated fraction after the HPE. This recovery period was characterized by a return of CN concentrations to near mean values, with continued low activated fractions. This suggests that the new particles formed during the HPE do not

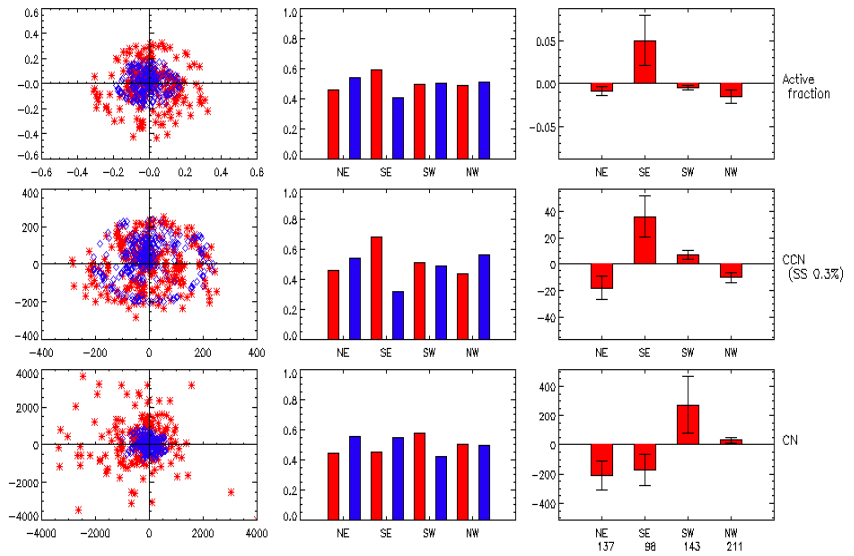

Figure 2.5: Positive anomalies (Red) and Negative anomalies (Blue) for activated fraction (top), CCN (cm^{-3}, middle) and CN (cm^{-3} bottom)

immediately go on to become CCN. This observation goes in support of the findings from Levin et al (2011); after the SPE there was an observed decrease in CN coincident with an increase in median diameter, but no immediate increase in CCN. They attributed the inverse relationship between CN and median diameter to coagulation, which, in all likelihood, is occurring during the HPEs observed at MVNP. However, despite the increases in aerosol size, these particles are new and mostly organic in nature (Levin et al. 2011), so they are associated with lower κ values and potentially less likely to serve as CCN under the low to moderate supersaturation environments (0.1 – 0.4% associated with updraft speeds ~1 ms^{-1} [Korolev and Mazin, 2003]) likely seen in stable orographic clouds. This explains the persistence of low observed activated fractions (ss=0.3%,ss=0.5%) after the observed HPEs.

The implication of this analysis is that close proximity SOA formation has a negligible effect on CCN. Furthermore, HPEs are observed much less often during the winter than they are the summer (Levin et al. 2011), so their relevance to wintertime orographic clouds is even less.

2.3: Aerosol and wind regimes

In Ward et al. (2010) an attempt was made to characterize aerosol regimes as related to wind direction. They found higher (though not statistically significant) CCN concentrations when the meteorological wind was from the southeast, along with higher CN concentrations and lower activated fractions. They speculated that freshly nucleated particles (too small to activate as CCN) originating from the pollution sources to the southeast of the sampling site were being measured. A similar, more thorough analysis is presented here.

The left panels of Fig.2.5 show anomalies (based on the observed averages, positive in red and negative in blue) for CN, CCN (ss=0.3%) and AF (from bottom to top), plotted on a wind rose. The center panels show the percentage of positive anomalies (red) and negative anomalies (blue) binned by quadrant, and the right panels show the average anomalies for each

quadrant, with error bars representing the mean ± 1 standard deviation. Positive CN anomalies appear to be larger in magnitude than negative anomalies in all wind quadrants, with the largest positive anomalies occurring when the wind direction is out of the west. The number of positive CN anomalies is greater than the number of negative anomalies in the western wind quadrants. Conversely, a higher number of negative CN anomalies were observed in the eastern wind quadrants. Despite more negative CN anomalies, there are a substantially higher number of positive CCN anomalies in the SE quadrant vs. all other quadrants. This is correspondent with a higher number of positive AF anomalies in this wind quadrant. These results are in direct contradiction to the findings presented by Ward et al. (2010). This discrepancy can be explained by how the data were analyzed.

During ISPA-III the meteorological data were recorded every hour, and the aerosol data every half hour, so there had to be some selection of how to match these data up for comparison. In the analysis performed here, only aerosol observations taken at the same time as the meteorological observations were used, the half hourly data were not included. In the analysis performed by Ward et al. the analysis was performed on a two-point average of the CCN data closest to the wind observation, e.g., the CCN data for the 1:00 wind observation was the average of the CCN data from 1:00-1:30. It seems more appropriate to use only the aerosol observations taken concurrently with meteorological observations vs. using a mean, because for each two-point mean, half of the average value is potentially associated with a different wind direction than the one being compared to. Taking only the data concurrent with wind observations not only simplifies the analysis, but also provides more confidence in the results. The remaining discussion will focus on the results found using aerosol data concurrent with wind observations.

The higher observed mean CCN and AF in the SE quadrant were statistically significant

above the 95% confidence level using a two-tailed comparison t-test between the mean in the SE bin to the total mean. No other wind regime showed statistical significance for CCN or AF, though the NE/SW showed statistically significant low/high means in CN concentration.

It is possible that, under southeast winds, there is a greater anthropogenic component to the aerosols observed at MVNP. This would suggest that the aerosol originating from the Four Corners power plant to the immediate southeast had a greater hygroscopicity than aerosols originating from the other three quadrants. Furthermore, SOA formation and growth occurs on short timescales near pollution centers (Volkamer et al. 2006). This would suggest aerosol originating from the Four Corners power plant to the southeast of MVNP may have grown to sizes sufficiently large to serve as CCN by the time they reached MVNP. These two physical explanations can account for the higher activated fractions observed under southeast winds. However, it is possible that when the winds are strong out of the southeast, a reduced activated fraction could be observed due to the presence of a large number of small aerosol particles that have not had sufficient time to grow to sizes large enough to be cloud active. This scenario would be more in line with the explanation from Ward et al.

While this analysis can provide some insight as to the observed aerosol properties at MVNP as they relate to the regional meteorological conditions, the results should be viewed with caution. Despite there being significance in the data, the fact that marginally different data analysis techniques yielded vastly different results reduces the confidence in these findings. Additionally, the highly complex topography around MVNP could potentially have affected the wind, and the wind measured at MVNP may not have always been representative of mean synoptic wind within the region. Additionally, the abundance of vegetation and the presence of dry loose soil at MVNP suggest that the observed CN and CCN concentration at was likely

influenced in part from the local natural sources from within the park.

2.4: Total SOA Burden on aerosol properties on the western slope.

An attempt was made to estimate the contribution of SOA on aerosol mass, size and concentration to the aerosol observed at MVNP. This was done by using measurements from both IMPROVE and ISPA-III. The upper limit of the SOA contribution to the total aerosol mass burden was estimated by: 1st, assuming all Organic Carbon (OC) measured by IMPROVE is SOA, and 2nd, removing OC mass from the total aerosol mass and comparing the difference. Using this method, ballpark estimates of the SOA contribution to aerosol concentration, size, and chemistry were found after making a few basic assumptions and using averages from the data collected at MVNP.

A new κ value is easily obtained using Equation 6 from Petters and Kriedenweis (2008), only now neglecting the contribution of OC. Aerosol size change estimates were computed by fixing the aerosol number concentration to the mean value (1781 cm^{-3}) observed a MVNP during the ISPA-III campaign. The size changes were then calculated by using Equation 10 from Saleeby and Cotton (2004) which relates aerosol size, mass, and number concentration for a fixed size distribution. Differences in concentration were calculated by simply inverting Equation 10 from Saleeby and Cotton, and using a fixed aerosol size of 20 nm as the input median diameter. The underlying physical assumption made for this analysis, was that 50% of the OC went into making new particles, and 50% went into making larger particles. Fig.2.6 shows the results of this analysis. Not surprisingly, the largest differences occur during the summer months, with the removal of OC reducing the estimates in median diameter and number concentration of ~15nm and ~200 (cm^{-3}), respectively. κ is also increased on average by 0.15

during the summer. During the winter however, the differences are much less severe, with reductions in median diameter and number concentration of only 5nm and 50 (cm^{-3}) (<5% of the mean CN concentration), and increases of κ less than 0.1. Additionally, the variance in the data is generally larger during the summer than in the winter, which suggests that the contribution from SOA during the winter is, for the most part, constant. It should be noted that the seasonal trend of the contribution of OC on aerosol size is consistent with the seasonal trend in aerosol size changes found by Levin et al. (2011), bolstering confidence in this analysis. Furthermore, with regards to the ability for aerosol to serve as CCN, there are competing influences that arise when removing OC. While the removal of OC causes underestimates in number concentration and in size, it causes overestimates in hygroscopicity. So, the overall contribution of SOA to CCN is probably even less, during the winter, than the 5% estimate above, as the overestimates in hygroscopicity of the aerosol will somewhat compensate for the underestimates of median diameter and lower number concentrations.

Based upon these results, the overall contribution of SOA to CCN during the winter months is in all likelihood small, if not negligible. This is in line with the previous research discussed in the literature review. Based upon these conclusions, parameterizing only primary CCN emissions within RAMS seems a reasonable alternative to using output from WRF-CHEM to nudge atmospheric aerosol concentrations, at least for model simulations of wintertime cases.

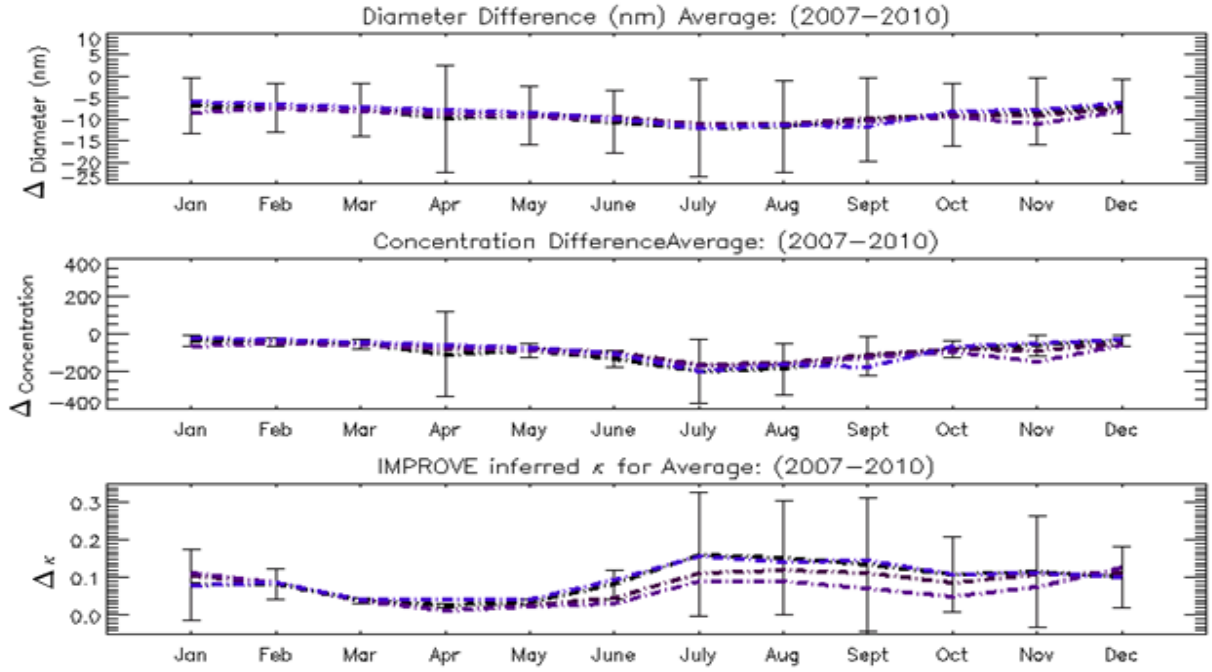

Figure 2.6: Estimated changes in aerosol median diameter (Top), aerosol concentration (middle) and kappa (bottom) without OC, derived from IMPROVE data.

Chapter 3: Aerosol Emissions Scheme

3.1: Aerosol Source Mapping

One of the major disadvantages of the aerosol nudging scheme developed by Ward et al. (2011) was that case-specific WRF aerosol output was required for all vertical levels. Another major deficiency was that the model domain in RAMS had to be identical to the domain used in WRF in all three spatial dimensions. These requirements severely limited this schemes utility. For one, WRF does not allow for user-prescribed vertical levels when nudging from real data, instead the vertical levels in WRF are fixed to that of the parent dataset. This places a restraint on the vertical resolution used in RAMS, limiting the number of vertical levels to typically <30. Additionally, performing nested simulations in WRF-CHEM with NEI anthropogenic emissions and MEGAN biogenic emissions is a complex and time-consuming process. Due to these complexities, Ward et al. opted to simply perform separate WRF-CHEM simulations that fit the RAMS parent and nested grids. This method generated aerosol nudge files for nested RAMS simulations. However, there were some problems with this method. One of the more significant problems was that the smaller WRF simulation did not include pollution from outside of the domain. As a result, the aerosol fields produced by each WRF simulation looked drastically different, despite the fact that they were for the same case study.

Other complications associated with the Ward et al. aerosol prediction scheme include inconsistencies in model physics between WRF and RAMS. For example, the two models maybe produce precipitation in different locations, so the aerosol is scavenged in one model simulation, and an not in the other. While both of these complications can lead to unrealistic aerosol fields within RAMS, the poor representation of cloud scavenging in WRF is thought to be the most problematic (Ward et al. 2011). It was suggested by Ward et al. that these problems

could be mitigated by running RAMS interactively coupled with WRF-CHEM. An interactive scheme would use WRF aerosol output to nudge the RAMS aerosol, which would then, in turn, nudge the WRF aerosol. While such a scheme may eliminate some of the errors associated with the Ward et al. method, it does nothing to address the increased computational expense associated with WRF-CHEM. Furthermore, the requirement that a full WRF-CHEM simulation is required (including a full 24 hour spin up period) for every RAMS grid makes any method that uses case-dependent WRF-CHEM output very time consuming. It is because of these deficiencies that creating an aerosol emission scheme that is confined entirely within RAMS is advantageous compared to the Ward et al. method.

The method proposed here for sourcing aerosol into RAMS is not altogether dissimilar to the method used by Ward et al., at least from a logistical standpoint. The aerosol sources are tied to an aerosol nudge file that matches the grid dimensions of the RAMS domain, similar to Ward et al. The differences lay in the generation and use of the nudge file. In the Ward et al. scheme, periodic output from WRF-CHEM is used to generate 3D nudge files, which nudge the aerosol (concentration, κ, and median radius)

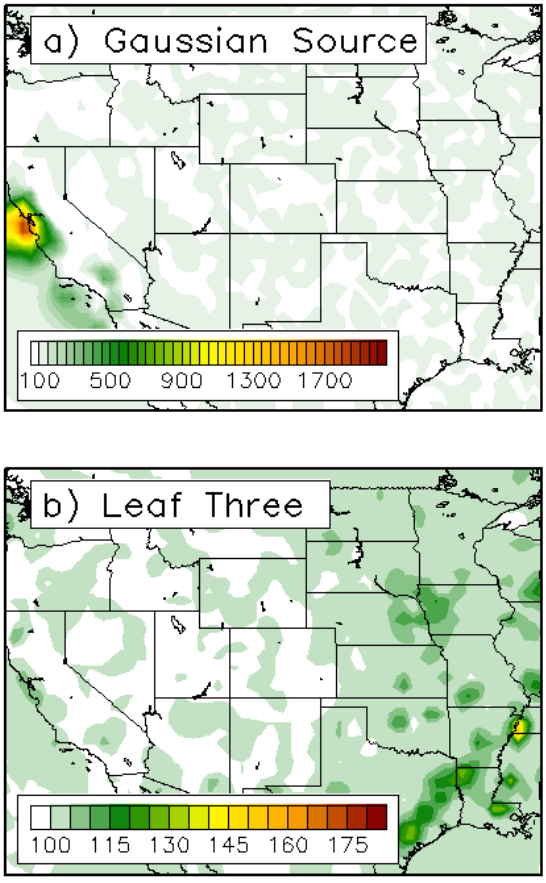

Figure 3.1: Surface aerosol concentration [cm^{-3}] 30 minutes after model initialization

in RAMS at all i,j,k grid-boxes. In the scheme presented here, a single 2D nudge file is created on the first time-step of a RAMS simulation. This nudge file is then used to nudge aerosol number concentration and κ at a fixed height (z_e) on the horizontal plane. There are two methods by which this nudge-file can be created. The first and simplest way is to prescribe a set of aerosol sources that are given the shape of a two-dimensional Gaussian distribution (an example is shown in Fig.3.1 a). This information is used to generate an aerosol nudge file for the parent grid, as well as each nested grid, that matches the domain of the RAMS simulation. This is a very simple, yet very powerful tool. It requires very little time, and it provides the user with a high level of control regarding the placement, size, and strength of any number of aerosol sources within the domain.

The second option uses bilinear interpolation to interpolate a gridded file to the RAMS domain. This is the option that makes it possible to use aerosol output from WRF-CHEM to act as the source map for the RAMS domain without the requirement of identical domain characteristics. This is very advantageous, as a single WRF simulation could provide an aerosol nudge file for an unspecified number of RAMS simulations. Another positive quality of this method is its adaptability. For example, while the research performed here uses output from WRF-CHEM to prescribe aerosol sources, it is possible to use other data sets, such as model output from the Goddard Earth Observing System (GEOS) chemistry model, or observational data from IMPROVE.

There is a third option to prescribe aerosol sources in RAMS that differs from the two options discussed above in that it neither generates nor requires a nudge-file. This method simply adds aerosol particles into the model as a function of urban and vegetation fraction as determined by the LEAF-3 surface model in RAMS (similar to Carrio and Cotton, 2008). This

option takes a user-prescribed maximum aerosol concentration (corresponding to a grid cell that is 100% urban) and sources aerosol into the model based upon the urban fraction. Emissions from the non-urban (vegetated) grid-cells are also relative to the maximum, user-prescribed, aerosol concentration, and loosely based on the method used in MEGAN, calculating an emission factor based on plant type, temperature and fractional coverage. The temperature dependence currently built into this scheme is based upon a linear relationship (r^2~0.25) between temperature and isoprene emissions found from WRF-CHEM output from one simulation. The dependence on plant type is based upon the listed dependencies from Guenther et al. (2006). Any plant category in RAMS that is not listed in Guenther et al. is given an emission factor of zero. Tying an aerosol emission rate to the vegetated grid-fraction from the leaf-3 model in RAMS provides an ad hoc representation of SOA formed from biogenic sources in RAMS. While a couple of quick test simulations using this method seem to produce reasonable looking aerosol fields (Fig 3.1 b), with most of the aerosol concentrated over urban areas, the values seem highly suspect (one to two orders of magnitude lower than expected), so this method is not preferable compared to the other two presented here.

The three methods presented here are all made available in RAMS, complete with flags and options in the RAMSIN namelist. This provides future users with a very high degree of control over aerosol sources within RAMS. However, the development of a source mapping scheme in RAMS is not the only challenge. There were still several obstacles that needed to be addressed before there was a fully functioning emissions scheme, including the representation of aerosol hygroscopicity, emission height, and emission method.

3.2: Aerosol Hygroscopicity

Until recently, aerosol chemistry in RAMS was prescribed in a very rudimentary manner. The original nucleation look-up-tables developed by Saleeby et al. (2004) assumed that all aerosols in RAMS were ammonium sulfate. A further upgrade to the look-up-tables for RAMS allowed for the inclusion of κ as an input variable so to represent aerosol chemistry. (Ward et al. 2011). Ward et al. made this upgrade specifically so that RAMS would work with output from WRF-CHEM, as κ can be explicitly calculated from this output. κ is an extremely valuable number to know. It is essentially a very simple way to represent the Kohler equations for aerosol water activity, which makes it highly attractive for numerical models. Furthermore, κ has known values for a large number of chemical species, which makes it quite simple to calculate a κ value as long as there is some information regarding the relative contributions of the different chemical species that make up the aerosol.

Unfortunately the κ look-up-tables were unique to the version of RAMS used by Ward et al. The most recent version, RAMS 6.1, still only used water-solubility as a means to represent aerosol chemistry. This meant that the first order of business was to adapt the look-up-tables from Ward et al. to the RAMS 6.1 framework. The κ look-up-tables did not outright replace the water-solubility look-up-tables; instead, a flag in the RAMSIN namelist was added, giving the user the option of using either κ or water-solubility.

Once the new look-up-tables were adapted to RAMS 6.1, the code had to be modified such that κ was treated as a three-dimensional scalar, rather than a fixed value for the entire domain. Changing κ into a 3D variable allows for the inclusion of a basic source dependent aerosol chemistry parameterization that goes along with the aerosol source map. In this

parameterization, κ is modified every time-step aerosol is sourced into the model, by simply taking a weighted-average of the newly added aerosol and the aerosol already in place. This is equivalent to the volume-weighted average from Petters and Kreidenweis (2007) as the aerosol size and density are assumed constant.

Once κ is adjusted, it is treated in the model as a passive tracer that is used only in the nucleation look-up-tables to calculate an activated aerosol fraction. The value of this variable does not change when aerosol are nucleated. For example, if some portion of aerosol with a κ value of 0.4 is activated and converted into cloud droplets, the aerosol concentration and mass will decrease, but κ will remain 0.4. This might be somewhat unphysical, as (all else being equal) κ should decrease slightly in nucleation scenarios as water will preferentially condense on to more hygroscopic aerosol. In addition to the unphysical treatment of κ during aerosol nucleation, the treatment of κ as a scalar array allows for its value to change artificially due to divergence. To keep κ values in check, upper\lower bounds, corresponding to the maximum/minimum value of κ in the nudge file were prescribed within the model. These bounds greatly mitigate the effects of divergence on κ. Despite these misrepresentations in the model, including κ as 3D variable allows for the inclusion of basic chemistry within the model, and ties aerosol hygroscopicity to pollution sources. Additionally, the errors described here generally do not overshadow the influence of the different aerosol sources.

3.3: Sourcing Aerosol into the Model

At first glance, sourcing aerosol into an atmospheric model sounds trivial, but there are a few different methods of doing this that exist in the literature. This section will focus on two

different methods of sourcing aerosol into the model and outline how they can be represented in RAMS. This section will also briefly discuss some of the physical assumptions made in each method as well as some of the potential pitfalls associated with them.

The inspiration behind the two emissions schemes described here stem from most widely described methods that have been used in the past to source CCN into atmospheric models. While the details of each emissions scheme vary, the overall goal is the same; add aerosol into the model.

Perhaps the most obvious method involves simply sourcing aerosol into the model at a fixed rate (ds/dt) (Eq.3.1). This method can be complicated by introducing dependencies on environmental variables such as temperature, windspeed, or time-of-day, though, as part of this research, no such dependencies are introduced. The most positive aspect of this method is that it is a physical representation of emission. An emission rate is a measurable quantity related to a physical dimension (time), and therefore using it in a model is highly representative of nature. There are, however, a few drawbacks associated with this method. The most salient drawback is source concentration error. Since there is no bound on how much aerosol can be sourced into the model, errors in the model emission rate can lead to large overestimates (underestimates) in domain total aerosol. Furthermore, without limiting the rate at which aerosol is sourced into the model there is a greater chance for the aerosol concentrations to become numerically unstable. Despite these errors, and because emission rates are physically understandable, this method is the most widely used in atmospheric chemistry models.

The second method described here removes potential errors due to inaccurate emission rates, or a poor representation of SA, but is also not a physically representative process. This method involves adding aerosol into the model by nudging the aerosol concentration at each grid

point towards a maximum value (Eq.3.2). This method is useful as it places an upper limit on the amount of aerosol that can be added into the model at each time step. Essentially this method allows aerosol sources in the model to be nearly constant in time, which better represents average aerosol concentrations over the sources. The major weakness of this method is that, once the aerosol number concentrations approach the maximum values at each grid point, the spatial distribution of aerosol becomes somewhat constant in time. Another problem that arises when using this method is that large increases in emission rate can occur in areas in which clouds and precipitation scavenge the aerosol. Lastly, this method is not a physical representation. Instead of basing the emission rate on a measurable quantity, the emission rate is based on the ambient aerosol concentration and an arbitrary nudging factor (generally around ~0.05). These drawbacks are what make this emission scheme less desirable than the constant rate scheme. However, this method has been used before and with reasonable success.

Carrio and Cotton (2008) used this method to source aerosol into the RAMS in order to study the effects of urban aerosol on convection. This paper studied how sea-breeze thunderstorms near Houston, TX interacted with increased CCN concentrations associated with the urban air-mass from the city. Because the nudging scheme limited the amount of aerosol sourced into the model, and because it generated fairly static aerosol fields, the effects of the urban aerosol could be isolated to storms that interacted with the city centers, corresponding to the goals of their paper. In cases such as this, it makes more sense to use a nudging scheme instead of a constant emission rate, as transport of aerosol from remote sources are not of interest, and may in fact serve to dilute the results. Because anthropogenic aerosol from remote sources (e.g., pollution centers on the U.S. west coast) is potentially important to the microphysical structure of orographic clouds in the mountains of Colorado, a constant emission

rate is more appropriate for the scientific goals of this thesis. However, since a larger goal of this thesis is to develop parameterizations of aerosol emission in RAMS for future studies, both of these methods were made available for use.

Regardless of which method is used, the prognostic variables are aerosol number concentration and κ. Aerosol mass is calculated from the number concentration using the same equation that initializes aerosol mass in the model, which assumes a fixed size distribution with a fixed aerosol median radius.

To save computational expense, the user has the option of determining how often to source aerosol into the model. There is a balance to be struck, as sourcing aerosol less often greatly reduces the computational expense, but also reduces accuracy. A few short test simulations revealed that accuracy did not appear to be severely compromised, so long as aerosol is sourced at least once every 5 minute period. On a single grid using 30 second time-step, this reduces computational expense by a factor of 10 vs. sourcing aerosol every time-step. So, while the loss in accuracy is trivial, the computational savings are not.

$$ccn(i,j,k) = \frac{ds}{dt}(i,j) * \Delta t + ccn(i,j,k)$$

Equation 3.1: Potential CCN Emission based upon constant rate at each i,j put into level model level k

$$ccn(i,j,k) = n_{fac} * [source(i,j) - ccn(i,j,k)] + ccn(i,j,k)$$

Equation 3.2: Potential CCN Emission based upon nudging

3.4: Emission Height

Originally, the emissions parameterizations developed for RAMS as part of this research

only sourced aerosol into the lowest model level, as based on the approach by Carrio and Cotton (2008). However, test simulations quickly revealed that this method was not able produce a realistic result. The aerosol tended to stay only at the lowest vertical level, and did not mix up into or above the boundary layer. This produced average aerosol vertical profiles far different than what can be typically observed (Raga and Jonas 1994 and Delene and Deshler 2001). The general thought is that for the simulations described in Carrio and Cotton, the vertical motion associated with the convective storm updrafts was sufficient to loft aerosol from the surface into the clouds where they could alter the cloud microphysics. Whereas, the simulations performed here are cold season cases devoid of sufficient boundary layer mixing to loft aerosol far above the surface level. While this result does potentially provide some insight regarding the transport of anthropogenic aerosol during the cold season, this is certainly not an accurate representation of emissions. Often, point sources such as smoke stacks protrude several meters above the ground, e.g., the height of the smoke stack at the Four Corners power plant is 90m high (Mamane and Pueschel, 1980). Additionally, chemical reactions occurring within the boundary layer act to produce SA above the surface. In order to better represent the contribution of elevated point sources, boundary layer SA formation, and unresolved boundary layer mixing, a method to determine the emission height in RAMS was developed.

In atmospheric chemistry models, such as WRF-CHEM, the emission height is prescribed by making use of a "plume-rise" model. A plume-rise model takes a number of variables into account in order to determine what model level pollution is placed into. Plume rise models can be quite complex by taking into account variables that are unique to each emission source such as smoke stack height, turbulence, and emission velocity (Ward et al. 2011). The concepts behind the plume rise model helped serve as inspiration for the emissions parameterization used

in RAMS, though the RAMS parameterization is much simpler.

The addition of a complex plume rise model into RAMS would have been very difficult to implement, requiring specific information unique to each aerosol source, and requiring more computer resources to solve the often complicated equations. Instead of using a plume rise model in RAMS, a constant emission height (z_e) is prescribed and applies to all grid points within the model. The aerosol added to the model is then split into the two vertical levels surrounding z_e through basic linear interpolation. This splits equations 3.1 and 3.2 into equations 3.1 a/b and 3.2 a/b respectively. As seen from these equations, as the emission height (z_e) approaches the height (z(k)) they will reduce back to the original equations, which source all of the aerosol into the vertical level k. Conversely, as z_e approaches z(k+1), the aerosol will be sourced entirely into the k+1 model level. In the model, if z_e is set as lower than the first vertical level, all the aerosol will be sourced into the surface level.

A few test simulations using this method (with z_e=100m) produced more reasonable looking results, however much of the aerosol still remained at or below z_e. To better simulate the emission height in RAMS an option was added to the RAMSIN namelist that uses the top of the boundary layer as z_e.

This option uses Equation 3.3 (from Sørenson, and Rasmussen [1996]), which makes use of the Richardson number (R_i) to find the top of the boundary layer. In the RAMS emission scheme, the boundary layer top is set as the level which R_i=0.24. While there is some question regarding the accuracy of Equation 3.3 in determining the boundary layer top, for the purpose of finding an appropriate level to source aerosol into, this method is sufficient. To save computational expense, R_i is not computed for all model levels, instead it is computed at each level, starting at the surface, until the critical threshold is crossed. Once this threshold is crossed,

z_e is computed through the linear interpolation of R_i at the levels surrounding the threshold value.

This method significantly changes the structure of aerosol emission, as z_e is variable, both in time and space. Of the methods for determining emission height described here, this scheme is the most related to a plume rise model as it brings in dependencies on atmospheric stability and turbulence, but source specific information (e.g., smoke stack height) involved. The sensitivity that model predicted aerosol has to emission height will be examined later on in this chapter.

$$ccn(i,j,k) = \left[1 - \frac{z_e - z(k)}{z(k+1) - z(k)}\right] \frac{ds}{dt}(i,j) * \Delta t + ccn(i,j,k)$$
$$ccn(i,j,k+1) = \left[1 - \frac{z(k+1) - z_e}{z(k+1) - z(k)}\right] \frac{ds}{dt}(i,j) * \Delta t + ccn(i,j,k+1$$

Equation 3.1: Constant source emission, a) Emission at lower vertical level, b) Emission at upper vertical level. z_e denotes emission height in meters

$$ccn(i,j,k) = \left[1 - \frac{z_e - z(k)}{z(k+1) - z(k)}\right] source(i,j) - ccn(i,j,k) + ccn(i,j,k)$$
$$ccn(i,j,k+1) = \left[1 - \frac{z(k+1) - z_e}{z(k+1) - z(k)}\right] source(i,j) - ccn(i,j,k+1) + ccn(i,j,k)$$

Equation 3.2: Nudging source emission, a) Emission at lower vertical level, b) Emission at upper vertical level. z_e denotes emission height in meters

$$R_i = \frac{gz(\theta_z - \theta_s)}{u_z^2 + v_z^2}$$

Equation 3.3: Richardson Number (Ri) where subscript z denotes height AGL, and subscript s denotes surface height. From Sørenson, and Rasmussen [1996]

3.5: WRF-CHEM

As discussed previously, the WRF-CHEM model was used to prescribe the aerosol sources used in the RAMS model. WRF-CHEM couples the WRF model with several different modules that predict gas phase chemistry, gas-aerosol, and aerosol-aerosol interactions. WRF-CHEM is particularly powerful because it has the capability to use real world emission

inventories documented within the National Emissions Inventory (NEI) from the Environmental Protection Agency (EPA) to simulate anthropogenic pollution as well as the capability to simulate natural emissions from the Model Emissions of Gases and Aerosols from Nature (MEGAN). The modules described in this section determine how the gas and aerosol species emitted into the model interact with each other as they are transported throughout the model domain.

Gas phase chemistry within WRF-CHEM is predicted using the Regional Atmospheric Chemistry Model (RACM; Stockwell 1997). RACM includes 77 chemical species which are allowed to react in the atmosphere through 237 thermal, photolytic and oxidation reactions (Ward et al. 2011). These gas species are then allowed to interact with and form new aerosols within the Modal Aerosol Dynamics Model for Europe (MADE; Ackermann et al. 1998).

Aerosols in MADE are represented by two lognormal size distributions, Aiken and accumulation mode. The modes are allowed to interact with each other through coagulation where the size distributions overlap.

Aerosols are added to the model through both primary emission and secondary formation from the gas species output from RACM. However, only the Kulmala et al. (1998) parameterization of sulfuric acid nucleation is used to nucleate SA. This means that all new particles are made up of entirely sulfate. Aerosols within the model are allowed to grow by both condensation of chemical species in the gas phase and coagulation of aerosols. Condensation changes the aerosol size and mass while holding the concentration constant and coagulation changes the aerosol size and concentration while holding the mass constant. If the aerosols grow to sizes greater than 1μm they are placed into the coarse mode, and treated independently of the Aiken and accumulation mode size distributions.

While the WRF-CHEM model provides the capability to explicitly resolve both primary emissions and secondary formation of aerosol, as well as both anthropogenic and natural sources, the accuracy is somewhat limited by some of the assumptions made within the model.

One major limitation to the model is that the nucleation of new particles is only prescribed using sulfate. This has been shown in the past to produce low-biases in SA formation in rural areas, where much of the SA is formed from organic monoterpenes (McKeen et al. 2007). Additionally, the condensation of isoprene products is not included within the model. This likely leads to a large underestimation of the aerosol organic fraction (Ward et al. 2011). Another major limitation is the lack of aqueous phase (cloud) chemistry within the model. This is important to mention as there is some evidence that the majority of sulfate aerosol is generated through aqueous phase chemistry (Kanakidou et al. 2005). However, the lack of cloud chemistry might somewhat offset the over-prediction of sulfate resultant from the nucleation parameterization and an over estimation of SO_2 emissions (Chapman et al. 2009). Perhaps the biggest limitation of the model is that there is no in-cloud scavenging of aerosol when using WRF-CHEM with the modules described here. This implies that the model only wet deposits aerosol through precipitation beneath the cloud, leaving aerosols above the cloud base essentially immune to scavenging. This limits the ability for WRF-CHEM to accurately simulate cases with high rainfall amounts.

Despite these deficiencies, WRF-CHEM can provide valuable insight into the interactions between pollution and meteorology. Furthermore, it can be used as a base comparison for the proposed emissions parameterization in RAMS.

3.6: WRF-CHEM Emissions File

To build an emissions file for RAMS the WRF-CHEM model was run for one hour (12-13z September 27, 2009) on a domain covering the western half of the United States. The model was run on a polar stereographic grid with 120 grid points in x and 98 grid points in y. It was run with a grid spacing of 25 km. The domain was set up to cover much of the western US, including all of the major urban centers on the Pacific coast. The model was initialized using the North American Regional Reanalysis (NARR) dataset. The vertical structure of the model was made up of 30 σ levels with the Top Of Atmosphere (TOA) set to 100 hPa. Anthropogenic emissions were treated using the NEI2005 inventory, and biogenic emissions were prescribed using MEGAN.

After one simulation hour the near surface aerosol output (concentration and κ) was saved and used as a gridded source file for RAMS. Aerosol output after one hour was used so that aerosols would have ample time to form near pollution centers, but not be dispersed across the whole domain. This produced a reasonable aerosol source map to (based upon the proximity of high aerosol number concentrations to known pollution sources and cities) **(**Fig. 3.2**)**. Additionally, by only allowing WRF-CHEM to run for one hour, a vast majority of the problems and biases mentioned previously are not an issue, in particular, the problem of cloud scavenging.

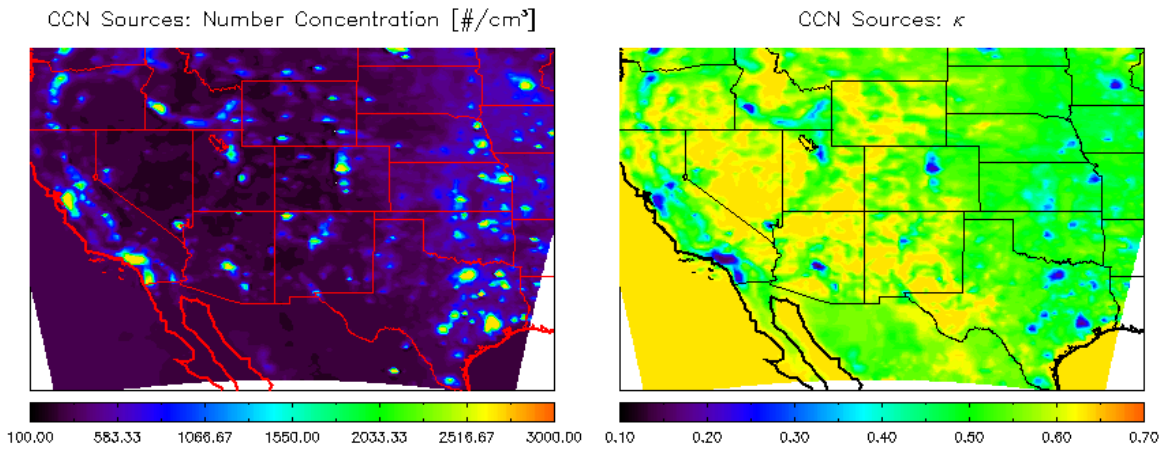

Figure 3.2: Aerosol source map generated after one hour of a WRF-CHEM simulation. Left: Emission Rate (#/hour), Right: κ

3.7: Test Simulations

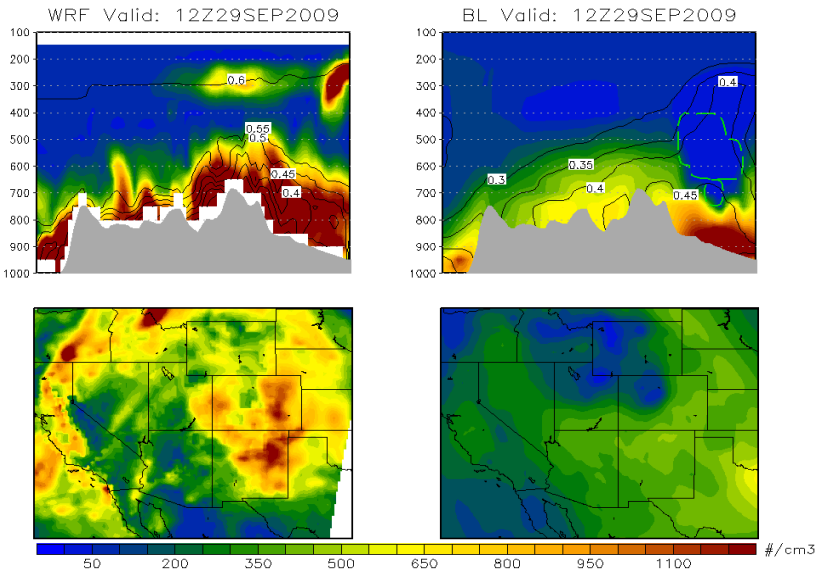

Figure 3.3: Near surface column average aerosol concentration (bottom) and EW cross section through 38.0 N (Top). Comparison between WRF and RAMS (green dash denotes cloud edge)

Test simulations in RAMS were run using the emissions file shown in Fig.3.3. The emissions were treated using the fixed rate method with the number concentration value at each grid point representing a per hour emission rate. Less rigorous simulations were performed using the nudging method. In general using this method

produced reasonable results, although the aerosol fields appeared tied to the sources, and relatively static in time compared to the constant rate method. Since the constant rate method appeared more representative of nature, this is the emissions method that will be discussed here.

The horizontal model set up in RAMS was the same as the *horizontal* set up used in WRF-CHEM for the generation of source files. In the *vertical*, RAMS was initialized with 35 vertical levels with stretched resolution ranging from 100m near the surface to 2km higher up. Three simulations were run using RAMS and one simulation was run using WRF-CHEM (WRF). The three RAMS simulations were run using aerosol emissions while varying $z_{e.}$ The aerosol vertical profiles were compared to that of WRF, and to known/observed profiles available from the previous literature. The emission heights used were a) the surface layer, (SFC) b) 100 meters above the surface (100m), 3) the top of boundary layer (BL). To compare these different emission options, the same test case was run using each option (September 27th 2009). For all of the RAMS simulations, the emission and transport of aerosol show reasonable looking solutions. In general, the aerosol concentrations tend to maximize around pollution centers and move with the synoptic flow. Furthermore, the aerosol concentrations were stable and never exceeded unreasonable values. A comparison between the RAMS BL simulation and the WRF simulation is shown in Fig. 3.3. This figure is representative of a snapshot 36 hours into the model simulations and serves as an example showing that RAMS compares reasonably well with WRF-CHEM. Both in RAMS and WRF-CHEM, the aerosol concentrations are highest east of the Colorado Front Range, with the majority of aerosol below 700hPa. Both WRF and RAMS show a relative maximum in aerosol concentration over north central New Mexico. The largest differences between RAMS and WRF-CHEM seem to be located in areas where there are clouds. This is simply because RAMS incorporates cloud scavenging and WRF-CHEM does not. While

all of the RAMS simulations show reasonable comparison to WRF-CHEM, the differences between the three RAMS simulations are more subtle. These differences are best shown by looking at the vertical distribution of aerosol.

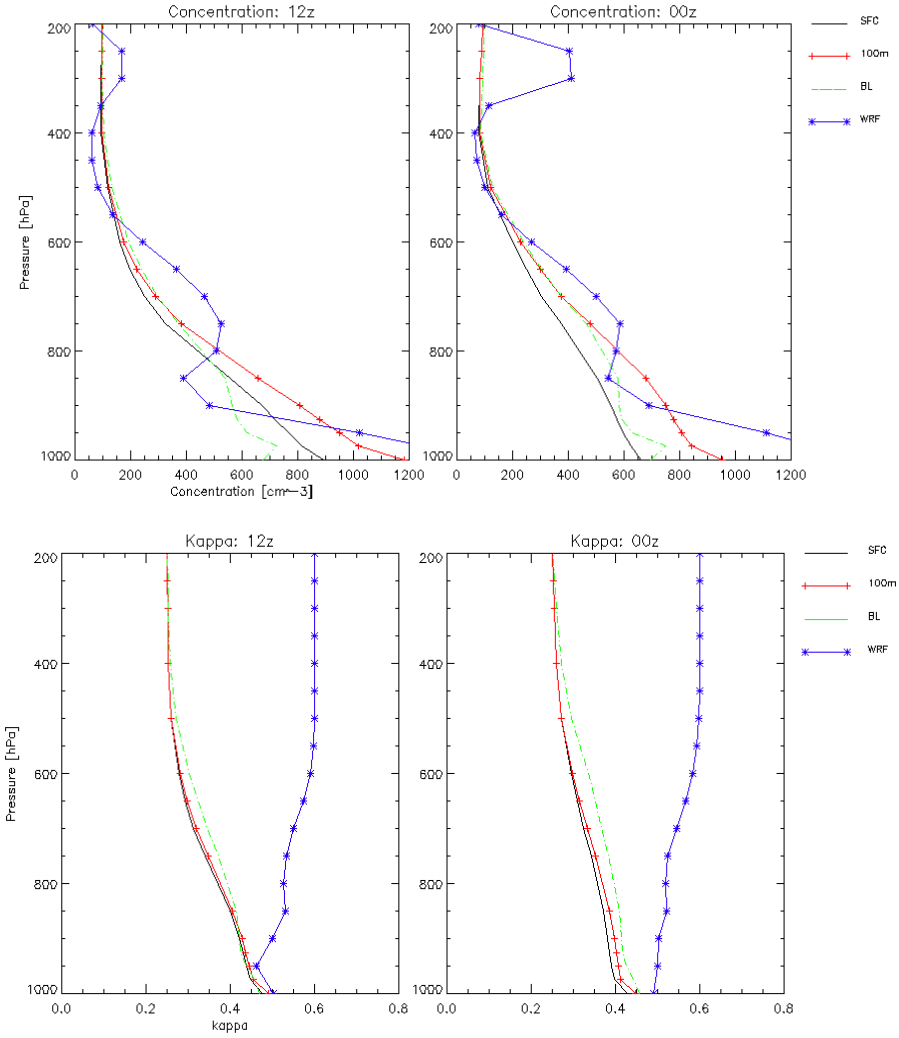

Figure 3.4: Top (a): Domain averaged aerosol concentration. Bottom (b) domain averaged κ.

Domain-averaged vertical profiles for each of the three RAMS simulations and the WRF simulation are shown in Fig. 3.4(a). One vertical profile is representative of an early morning profile and another of early evening (12 UTC Sep 29 and 00 UTC Sep 29, 36 and 48 hours into the model simulation). This was done to show diurnal variations associated with the development of the convective boundary layer. It can be seen that there is not a large qualitative difference between the z_e=SFC, z_e=100m, and z_e=BL. In all cases the aerosol appears somewhat well mixed in the lower troposphere, before a rapid decrease to lower concentrations in the upper troposphere. The BL

simulations overall add less aerosol into the model, but do generate slightly higher aerosol concentrations above ~700hPa. The BL simulations also have a maximum aerosol concentration slightly above the surface, whereas the 100m and SFC concentrations always decrease with height.

Both the 100m and BL cases show better qualitative similarities to the vertical profiles measured by Delene and Deshler (2001) and Raga and Jonas (1994) than the SFC case, with the 100m simulation appearing the most similar. Furthermore, these profiles look more similar to the vertical profile produced by WRF-CHEM, though there is more variability in WRF Chem, likely a result of SA formation. WRF-CHEM also produces a smaller secondary maximum in concentration near the tropopause. This is probably the model representation of the famed "Junge Layer" (Junge et al. 1961). This feature is not present in the RAMS simulations, which is not surprising as the aerosols within this layer are made up from SA (Junge et al. 1961). Since the Junge Layer is unimportant in relation to orographic snowstorms, the lack of its presence in RAMS is not of much concern.

Fig. 3.4(b) shows the vertical profile of κ for the three RAMS simulations and the WRF-CHEM simulation. The κ profiles in the RAMS simulations look very similar, with relatively high values of κ near the surface decreasing to more or less uniform values above ~850hPa. The BL and the 100m emission height simulations show higher κ values extending to greater altitudes than the SFC simulation. This is not a surprising result, as the more hygroscopic anthropogenic aerosol is emitted at higher altitudes in BL and 100m simulations. The WRF-CHEM κ profile behaves dissimilar to the RAMS simulations, with overall higher values of κ at all heights, and a general increase in κ with height. The vertical profiles of κ from RAMS are more similar to the vertical profiles presented by Pringle et al. (2010). This is somewhat

remarkable as this would suggest that the simple RAMS aerosol parameterization is seemingly able to simulate aerosol hygroscopicity better than WRF-CHEM. Though it should be mentioned that the vertical profiles of κ presented by Pringle et al. were also derived from model output, so whether or not κ in RAMS is more representative of the real environment vs. WRF cannot be definitively concluded. However, the model used by Pringle et al. did include a number of key chemical and microphysical processes not included in the WRF-CHEM simulations, so there is a higher degree of confidence in the Pringle et al. (2010) results.

The general overestimate of κ from WRF-CHEM can be traced back to the overestimate of sulfate aerosol fraction. The increase in κ with height in WRF-CHEM is simply attributed to the overabundance of nearly pure sulfate aerosol higher up in the atmosphere, where less hygroscopic (organic) gases and aerosol emitted from the surface cannot easily reach. This bias can be almost entirely explained by the parameterizations in WRF-CHEM as it does not properly form condensable from organic chemical species via photochemistry in the atmosphere, as is known to occur.

The overestimate of sulfate from WRF-CHEM is highly visible in the comparison between the WRF-CHEM model output and observational filter data from the IMPROVE network. The time period covered by the WRF simulation only covered one day of data collection from IMPROVE. To compare output from WRF-CHEM to IMPROVE, the surface mass ($\mu g/m^3$) concentrations of relevant aerosol chemical species were summed for the 24 hour period in WRF that coincided with the time the IMPROVE network collected data. WRF output was compared to IMRPOVE data at 11 IMPROVE sites across the western United States (Shown in Appendix 1). WRF-CHEM does not explicitly solve for ammonium sulfate [$NH_4(SO_4)$] and ammonium nitrate [$NH_4(NO_3)$]. The concentrations of these chemical species were calculated by

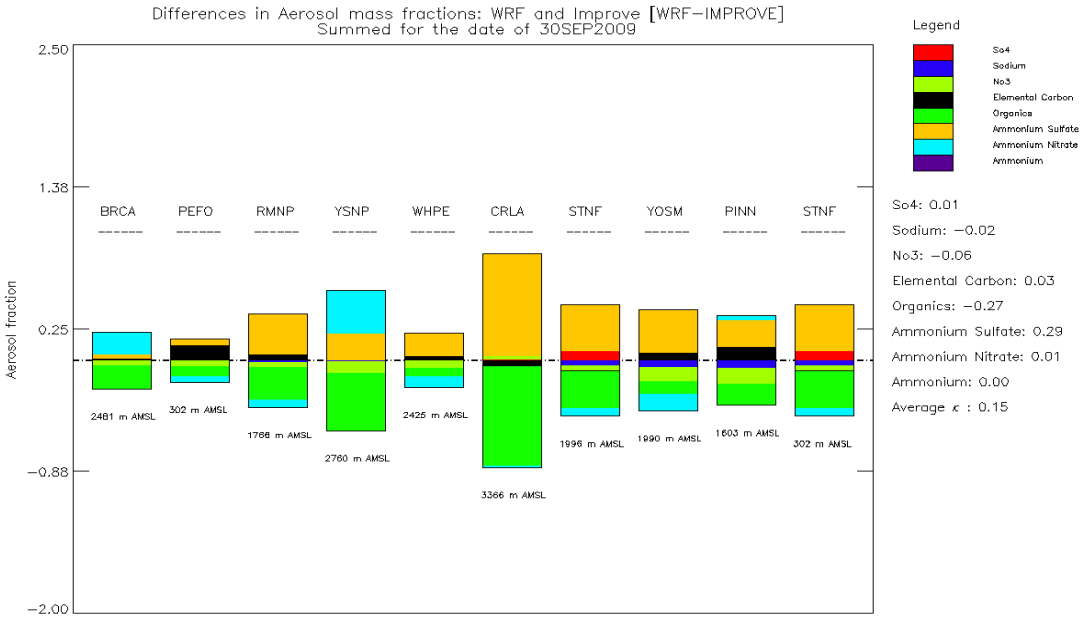

Figure 3.5:Differences in aerosol mass WRF-CHEM-IMPROVE

using the same method as Ward et al. (2011). This method uses the concentrations of sulfate, nitrate, and ammonium as input for the computation of $NH_4(SO_4)$ and $NH_4(NO_3)$. The major assumption made in this case that ammonium will preferentially combine with sulfate to form $NH_4(SO_4)$, and if there is any ammonium left over it will combine with nitrate to form $NH_4(NO_3)$ (Petters and Kreidenweis 2007). From here, it is a simple matter of using the chemical formulas to calculate concentrations of $NH_4(SO_4)$ and $NH_4(NO_3)$. These formulas pair two moles of ammonium to one mole of sulfate, and one mole of ammonium to one mole of nitrate. Once again, κ is computed by using Equation 6 from Petters and Kreidenweis.

In general WRF does not do qualitatively terrible in terms of capturing the basic trends in aerosol concentration. In both WRF and IMPROVE the sulfate aerosol species [including $NH_4(SO_4)$ and $NH_4(NO_3)$] account for most of the total aerosol mass. Additionally, in both WRF and IMPROVE, organic carbon is a larger contributor to aerosol mass than elemental carbon.

However, WRF vastly over-predicts the total aerosol mass, in some cases by nearly a factor of five, with the majority of this coming from over-predictions in sulfate mass.

Fig. 3.5 shows the differences in aerosol fraction (WRF-IMPROVE) for each location. From this figure it is seen that in all cases WRF-CHEM grossly over-predicts the fractional amounts of the more hygroscopic $NH_4(SO_4)$ and $NH_4(NO_3)$ aerosol species at all locations, which leads to large under-predictions of the organic aerosol fraction. This figure also shows under-predictions of sulfate from WRF, however this is an artifact left over after computing $NH_4(SO_4)$ and $NH_4(NO_3)$. The over-prediction of sulfate species from WRF-CHEM does not only cause over-predictions in aerosol mass and concentration, but also over-predictions in κ.

The difference in κ between WRF and IMPROVE ranges from -0.09 at the Petrified Forest (AZ) , to 0.45 at Crater Lake (OR), with an average of 0.08. The underestimate in κ at the Petrified Forest is associated with a small under-prediction of organic aerosol mass, coincident with a relatively large over-prediction of elemental carbon. The enormous overestimate of κ at Crater Lake is almost entirely caused by a very large model underestimate of fractional organic carbon. Subtracting this value from the average domain-averaged κ value (Fig.3.4(b)), brings the surface κ down to levels more consistent with RAMS and with the results from Pringle, et al. It was speculated by Ward et al. (2011), that the overestimate of κ by WRF-CHEM was potentially associated with underestimates in total organic aerosol mass. In this comparison no consistent underestimates in organic aerosol mass were found, and the over-prediction of aerosol hygroscopicity was most-tied to over-prediction of aerosol mass within sulfate species.

The test simulations described in this chapter serve as a proof of concept for the emissions scheme in RAMS. All of the RAMS simulations were able to produce reasonable

looking results, and agreed fairly well with WRF-CHEM. The 100m and BL simulations were able to loft aerosol above the boundary layer much more efficiently than the SFC simulation. The predicted κ from RAMS compares better to previous research and observations from IMPROVE than it does from WRF-CHEM, which is fairly remarkable.

These simulations suggest that this emissions parameterization used in RAMS is a reasonable alternative to using WRF-CHEM output to nudge aerosol values, the major benefits of this parameterization remain the reduction of computational cost, and the greater degree of user control. For example, the same 84 hour model simulation in RAMS took ~1.5 days vs. nearly 8 days for WRF. This is a cost reduction of ~550%, which is certainly a significant improvement. Additionally, because the schemes presented here remove the need for domain and case dependent WRF-CHEM output, it is much simpler to use. Lastly, because the schemes here are complete with RAMSIN flags and options, future users are given a high degree of control without having to edit the model code.

While this scheme is very valuable in terms of reducing computational expense, the test simulations performed here do not rigorously test the accuracy of it compared to observations. The next chapter will compare results from RAMS simulations using this scheme to aerosol data collected at MVNP during ISPA-III. As a comparison, the results will be compared to WRF-CHEM as well.

Chapter 4: Case-Studies

The aerosol emissions parameterization discussed in detail throughout the previous chapter was validated by using it in RAMS simulations of real case studies that fell within the measurement period of the ISPA-III field campaign. This was done by comparing the model output aerosol concentration at MVNP to the observations from ISPA-II. The difficulties in trying to validate an entire model by comparing it to measurements at a single geographical location cannot be understated. This was especially difficult for the analysis here, considering that the ISPA-III observations did not include explicit information relating to the aerosol size or chemistry. For additional validation, WRF-CHEM was run for the same case-studies. Running WRF-CHEM provided a base comparison for RAMS three-dimensional aerosol fields. Additionally, the WRF-CHEM output aerosol was also compared to the ISPA-III observations. This provided additional information regarding the accuracy of WRF-CHEM compared to RAMS.

4.1: Model description:

For the case studies discussed in this chapter, the RAMS model was set up using a single grid with 120 grid-points in x and 98 grid-points in y. It was given a horizontal grid-spacing of 25km in both x and y. The domain was centered on the location of MVNP, and covered the entire western United States. The model structure in the vertical was set up on the hybrid height-σ coordinate with 35 stretched vertical levels starting with a vertical resolution of 100m near the surface and ending with a resolution of 2km at its most coarse.

Both the North American Regional Reanalysis (NARR), and the National Center for Environmental Prediction (NCEP) reanalysis products were used to initialize and nudge the boundary conditions for the RAMS simulations. The reason both datasets were used was that,

after performing several simulations using the NARR, it was discovered that the RAMS 6.1 version had a technical issue associated with the NARR that resulted in a large under-prediction in precipitation. However, this technical issue revealed (somewhat serendipitously) features in the RAMS aerosol fields that were worth discussing.

Aerosol emissions in RAMS were treated using the constant rate scheme, with source mapping prescribed from the WRF-CHEM output file. Three RAMS simulations were run; one, a control (CTL) with a constant background aerosol concentration of 100 (cm^{-3}) and no aerosol emission, one with aerosol emissions at 100m (100m), and one with aerosol emission at the top of the boundary layer (BL).

Due to the relatively coarse resolution, in both the horizontal and the vertical, it was not expected that the model would be able to resolve any microphysical changes in the clouds resultant from CCN changes. This is not a large problem as the aim of simulating these cases was not to investigate the microphysical structure of clouds. Instead, the aim of these simulations was to compare model CCN concentrations to the observations at MVNP, and determine if RAMS is able to show reasonable temporal variability and transport of aerosol throughout the domain. As a check, one of the case-studies was run using three telescoping grids centered over MVNP. The results from the high resolution nested simulation did not differ substantially from the coarse resolution single grid simulation. Therefore, it was determined that, for the purposes of performing the case-studies discussed in this chapter, using a relatively coarse model set up to save computational resources was a reasonable approach.

In addition to running simulations in RAMS, WRF-CHEM was also run for these case-studies (thus the need for a computationally cheap model setup). The domain used in WRF-CHEM was very similar to the domain used in the RAMS simulations, except it was run on a

Lambert, instead of a polar stereographic projection. This made it easier to grid the NEI emissions properly. Aside from this small difference, the domain was the same 120x98 with 25km grid-spacing. The vertical coordinate used was the σ coordinate. The model was initialized and nudged every 6 hours using the NARR data set. The vertical structure of the NARR data set allowed for 30 vertical levels with a TOA set to 100hPa. The details of the model set-up for both RAMS and WRF-CHEM are shown in Table 4.1. In both case-studies each model simulation was given a spin-up time of 24 hours before the model output was analyzed, the same amount of spin up time used by Ward et al. (2011).

Table 4.1: RAMS and WRF-CHEM model set up for the 28 Sept 2009 and the 11 Oct 2009 Case-studies

RAMS		WRF-CHEM (ARW Core)	
Model Aspect	Setting	Model Aspect	Setting
Grid	120x98 Δx/Δy=25000(m)	Grid	120x98 Δx/Δy=25000(m)
Domain Center (Lat, Lon)	37.2, -108.4	Domain Center (Lat, Lon)	37.2, -108.4
Vertical Structure	35 vertical-levels: Δz: stretched from 100m at surface to a maximum of 2km Model-top: 15000m	Vertical Structure	30 vertical-levels σ-coordinate Model-top=100hPa
Initialization and Nudging	2.5º NCEP / 32.4km NARR Nudged every 6hr	Initialization and Nudging	32.4km NARR Nudged every 6hr
Radiation	Harrington	Radiation	LW: rrtm SW:Dudhia
Boundary Conditions	Klemp-Wilhemlson	Boundary Conditions	Mellor-Yamada-Janjic
Cumulus Parameterization	Kain-Fritsch	Cumulus Parameterization	Kain-Fritsch
Emissions	Constant Rate Emission File: WRF Aerosol File Z_e= 100m / Boundary Layer Nudge Frequency: 300s	Microphysics Scheme	Lin
		Chemistry Initialization/Nudging	Anthropogenic: NEI2005 Biogenic: MEGAN
		Chemistry Scheme	RACM, MADE/SORGAM
		Deposition/Scavenging	Dry Deposition: On Wet Scavenging: Off

4.2: Case 1: September 28 2009: 00 UTC – October 1st 12 UTC

4.2.1: Synoptic Overview

The 28 Sep – 1 Oct 2009 time period was chosen as a case study for several reasons. The most pertinent reason is that it was meteorologically active. A second reason this case was chosen was that orographic precipitation occurred on the Western Slope during this case-study, making it highly relevant to the eventual goal regarding the application of this emissions scheme. The evolution of the synoptic pattern that occurred over the western US throughout the time period within this case-study was as follows.

The weather that dominated over the western US at the beginning of the time period was best described as "fair." At the upper-levels a large area of high pressure dominated, with generally weak anti-cyclonic flow aloft. At the surface the temperatures were relatively mild, by late September standards, over much of the elevated terrain that makes up the inter-mountain west. The mean sea-level pressure pattern over the region best resembled that of a weak land-generated thermal low over the elevated terrain. However, to the northeast of the Rocky Mountains a strong area of high pressure associated with a moderately cold air-mass was building south across the Great Plains. This high pressure is significant as the model simulations suggest that it plays a role in transporting large amounts of pollution from the Texas coast into the Four Corners region. This will be explored in more detail later.

As time progressed, the upper-level ridge propagated eastward and amplified as it ran into the cold air-mass east of the Rockies. By 18 UTC on the 28th, the ridge axis was located directly above the ISPA-III observation site at MVNP. It was at this time that a moderately well amplified trough was starting to affect the Pacific Northwest. At the surface, the northerly winds and associated cold air east of the Rockies were present as far south as the Gulf coast where they intersected northeasterly return flow around the surface high. This return flow would advect air

from the southeast into the inter-mountain west region until ~18 UTC on the 29th when the zonal component of the surface wind shifted from easterly to westerly.

By 00 UTC 30 Sept the upper-level ridge had moved east of the Rockies ahead of an increasingly amplified trough. Winds aloft over the inter-mountain west were generally uniform out of the southwest. Precipitation associated with this storm was starting to impact the coastal regions of Washington and Oregon. By 06 UTC the trough had moved onshore and precipitation was starting to form along the mountain slope of Colorado ahead of the trough. This precipitation persisted on and off throughout the region until 18 UTC on the 30th as the trough drifted slowly northeast of the region. At the same time a very strong lee-cyclone was maturing along the Colorado/Wyoming border east of the Rockies. Strong cold air advection on the northwest side of the cyclone was affecting MVNP and the Colorado Western slope. As cold air advection strengthened and persisted along the Western Slope from 00-12 UTC 1 Oct, orographic precipitation started falling in the mountains. This precipitation persisted throughout the remainder of the case-study. The main meteorological aspect of this case-study was the development and passage of a synoptic wave through the inter-mountain west, including the Four Corners region. The ISPA-III meteorological observing station at MVNP recorded two significant wind shifts, a temperature drop associated with the cold front, and while no measurable precipitation was recorded at MVNP, nearby surface observations and RADAR data showed showers and thunderstorms in the vicinity.

The aerosol observations at ISPA-III also showed interesting trends. The CCN (ss=0.3%) showed a generally slow increase throughout the observed period, with notable increase and subsequent decrease that took place between 00 UTC 29 Sept and 00 UTC 30 Sept. This was coincident with the pattern shown in the CN observations indicating that there was no significant

change in activated fraction during this time. From 00 UTC to 12 UTC 30 Sept, the CN concentrations increased to their highest levels (~2500 cm^{-3}) before decreasing to around ~1500 (cm^{-3}) between 12 UTC 30 Sept and 06 UTC Oct 1. During this time, the CCN (ss=0.3%) remained generally constant, which indicates that the CCN activity was driven more by aerosol size and chemistry than it was by concentration. In order to best assess model performance regarding aerosol concentrations, it is most beneficial to compare times in which the aerosol activated fraction is generally constant. This is because the RAMS model assumes a constant aerosol radius, greatly reducing the dependence of aerosol activity to the aerosol physical properties in the model. In other words; time periods in which CCN concentrations vary coincident with CN concentrations are most likely to be simulated properly in RAMS, while time periods in which CCN concentrations vary coincident with activated fraction, are not likely to be represented well.

4.2.2: Model Performance

Overall, both the simulations initialized with NARR and NCEP data in RAMS as well as the WRF simulations performed qualitatively well in capturing the synoptic evolution of this case. All three simulations were able to properly simulate the propagation of the trough into the domain, and its accompanying lee-cyclone over the Western Great Plains. Additionally, all three models were able to accurately simulate the near surface return flow around a strong surface high during the first part of the case-study. RAMS initialized with the NCEP data seemed to perform slightly better than the simulation initialized with the NARR in terms of capturing the magnitude and timing of the synoptic wave passage across the region.

With regards to precipitation, the differences between the three simulations were more substantial, particularly the differences between the NARR and the NCEP simulations. The

RAMS simulation using the NARR to nudge the data did very poorly with respect to precipitation. In fact, the NARR simulation was not able to produce any reasonable amounts of precipitation throughout the entire case-study, whereas both the NCEP and WRF-CHEM simulations seemed to perform reasonably well. Both models were consistent with the timing and location of the frontal precipitation associated with the synoptic wave. Additionally, the NCEP and WRF-CHEM simulations were both able to produce orographic precipitation in the Rockies after 00 UTC 10 Oct, consistent with the observations. The NCEP simulation produced a spurious convective system that crossed the eastern part of the domain during the time period between 03 and 21 UTC 29 Sep.

The NCEP and the WRF-CHEM simulations did fairly well with the precipitation associated with the passage of the synoptic wave, both in terms of timing and location. The models did not match up exactly with the observations, but these were convective showers, so the fact that the models seemed to get the general location and coverage right is acceptable. Because all three model simulations seemed to be consistent across the board with respect to synoptic flow, both with each other and with the observed pattern, all three simulations can provide information relating to the transport of aerosol throughout the domain.

The next part of this chapter will compare the model output to the aerosol observations taken at MVNP, and then examine the model aerosol fields as they evolve with the synoptic pattern. The model's performance with regards to aerosol will be assessed by how well the model aerosol matches the observations at MVNP, and how consistent the models are relative to each other.

4.2.3: Assessment of model performance with respect to aerosol

The assessment of how well RAMS is able to simulate the evolution of atmospheric aerosol is a difficult task. However, the results of this case study appear encouraging. Fig. 4.1 shows the time-series of the RAMS simulations, the WRF-CHEM simulation, and the observed CCN (ss=0.3%). The model time-series values are taken from the surface level of the grid-point nearest to the latitude/longitude coordinate of the MVNP observing station. The mean difference between the model output and observed aerosol concentration at MVNP for each model is shown in Table 4.2. Fig. 4.1 and Table 4.2 serve as good illustrations of the problems associated with the WRF-CHEM model.

Table 4.2: Mean difference between observed and modeled CCN [# cm-3] for the 28 Sept 2009 Case

Simulation	**Mean**	**Standard Deviation**
Control (CTL)	-470.85	66.13
Z_e=100m (100m)	-175.29	121.35
Z_e=BL (BL)	-325.61	97.38
WRF	483.42	863.65

During the time period of the case-study leading up to the passage of the front, WRF-CHEM performs reasonably, although it does not seem to correlate with the observed variation of CCN at MVNP. Despite this, it produces reasonable aerosol number concentration values. At the time of the frontal passage, when the observed aerosol concentration at MVNP decreases rapidly, the predicted aerosol concentration from WRF-CHEM increases very rapidly to nearly double that of the observed. This result highlights the deficiency of using large scale fields of WRF-CHEM output to predict aerosol number concentration, especially in terms of orographic snowstorms. This overestimate (~2500 cm^{-3}) in aerosol concentration is occurring at the same

time that orographic precipitation is forming in the Colorado Rockies. As an example, by assuming an overestimate of ~2500 aerosol (cm^{-3}), and assuming an activated fraction of 0.3, the CCN concentration is overestimated by 750 (cm^{-3}). A comparison of this value to the results of Saleeby et al. (2008) suggests that this error in CCN could result in a ~ 6.5% loss of Snow Water Equivalent (SWE) on windward mountain slopes resultant purely from errors in the model predicted CCN concentration. RAMS seemed to perform much better than WRF-CHEM, although RAMS consistently underestimated the aerosol number concentration. It is possible that the low-bias in the RAMS predicted aerosol concentration could be associated with the lack of SA in the model, but this could not be definitively determined. The RAMS 100m NCEP simulation performed the best of all of the RAMS simulations, including the control. This is not

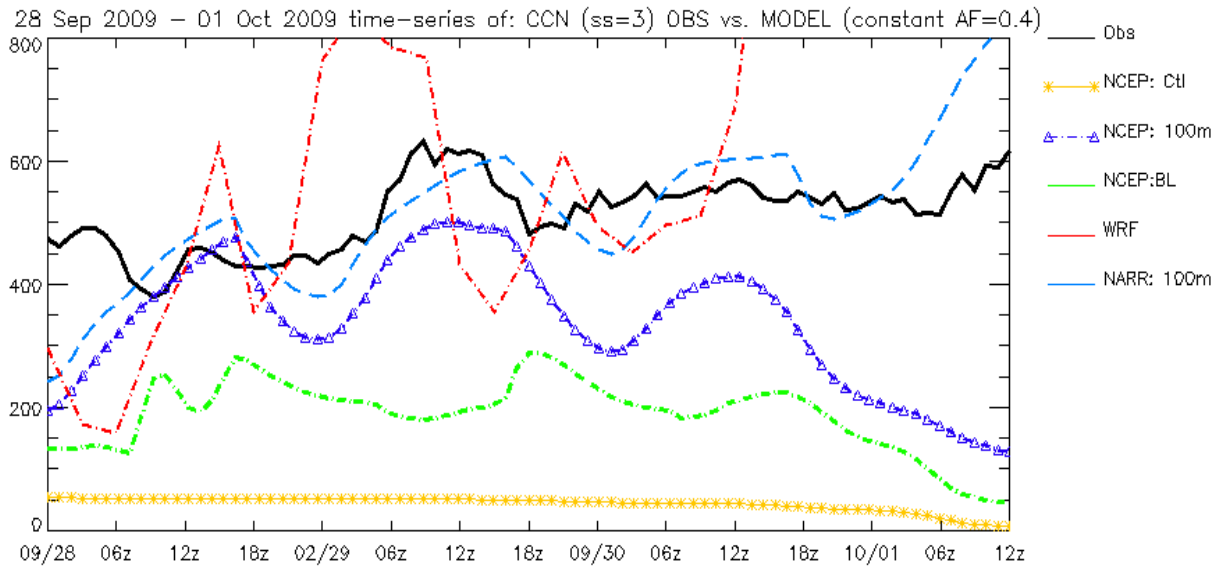

Figure 4.1: Observed CCN [# cm^{-3}] compared to the modeled CCN [# cm^{-3}] at MVNP, for each model simulation

surprising as the test simulations discussed in chapter three revealed that the using z_e=100m seem to produce the most realistic results. The rest of the analysis performed in this section will focus on the 100m RAMS simulations. The NARR simulation performed reasonably well throughout the majority of the case-study, but, similarly to WRF-CHEM, over predicted aerosol number concentration east of the synoptic trough towards the end of the case. This was attributed to the lack of precipitation and scavenging in the NARR simulation. The 100m NCEP simulation was able to (at least in some instances) correlate reasonably well with the observed aerosol. The best correlation occurred during 09/29 00 UTC – 09/30 00 UTC. During this time, the aerosol concentration increased while the aerosol activated fraction stayed relatively constant. This scenario is the most likely scenario to be well represented in RAMS. Because RAMS showed a very strong correlation during this time (r^2~0.6), it was worth investigating further.

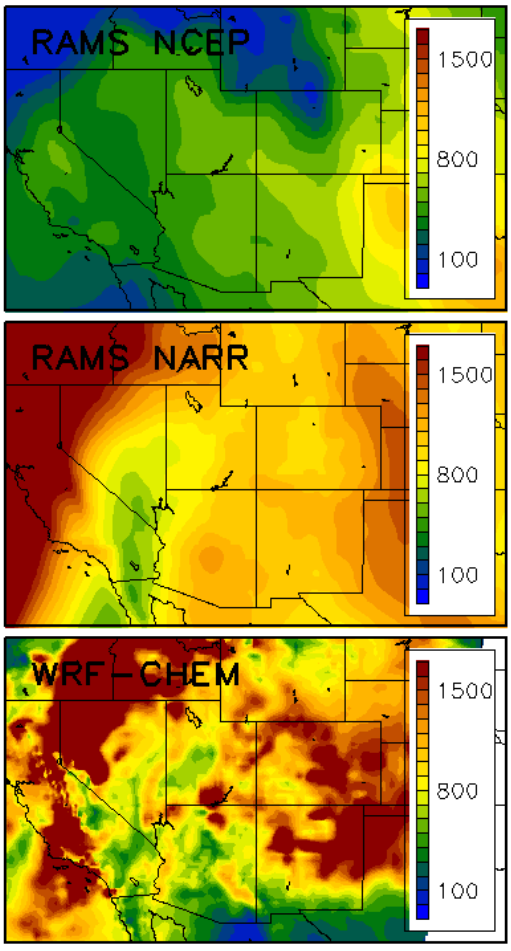

Figure 4.2: Comparison between RAMS and WRF-CHEM column averaged [# cm^{-3}] (between 1000-650hPa) at 15 UTC Sep 29

During the time period of 09/12 00 UTC and 09/30 00 UTC, the RAMS modeled aerosol fields showed a resemblance to the fields from WRF-CHEM, especially the NARR output (Fig. 4.2). Both RAMS and WRF-CHEM

model show relatively clean air being drawn in from the South Pacific Ocean to the southwest United States. They also show a relative maximum in aerosol concentration over northern New Mexico and the western Great Plains, although the NCEP simulation does not show this, due to aerosol scavenging from the spurious precipitation. There is also an area of high aerosol concentration in the Northwest corner of the domain, ahead of the synoptic trough, present in both RAMS and WRF-CHEM. It is highly encouraging that RAMS is able to capture features

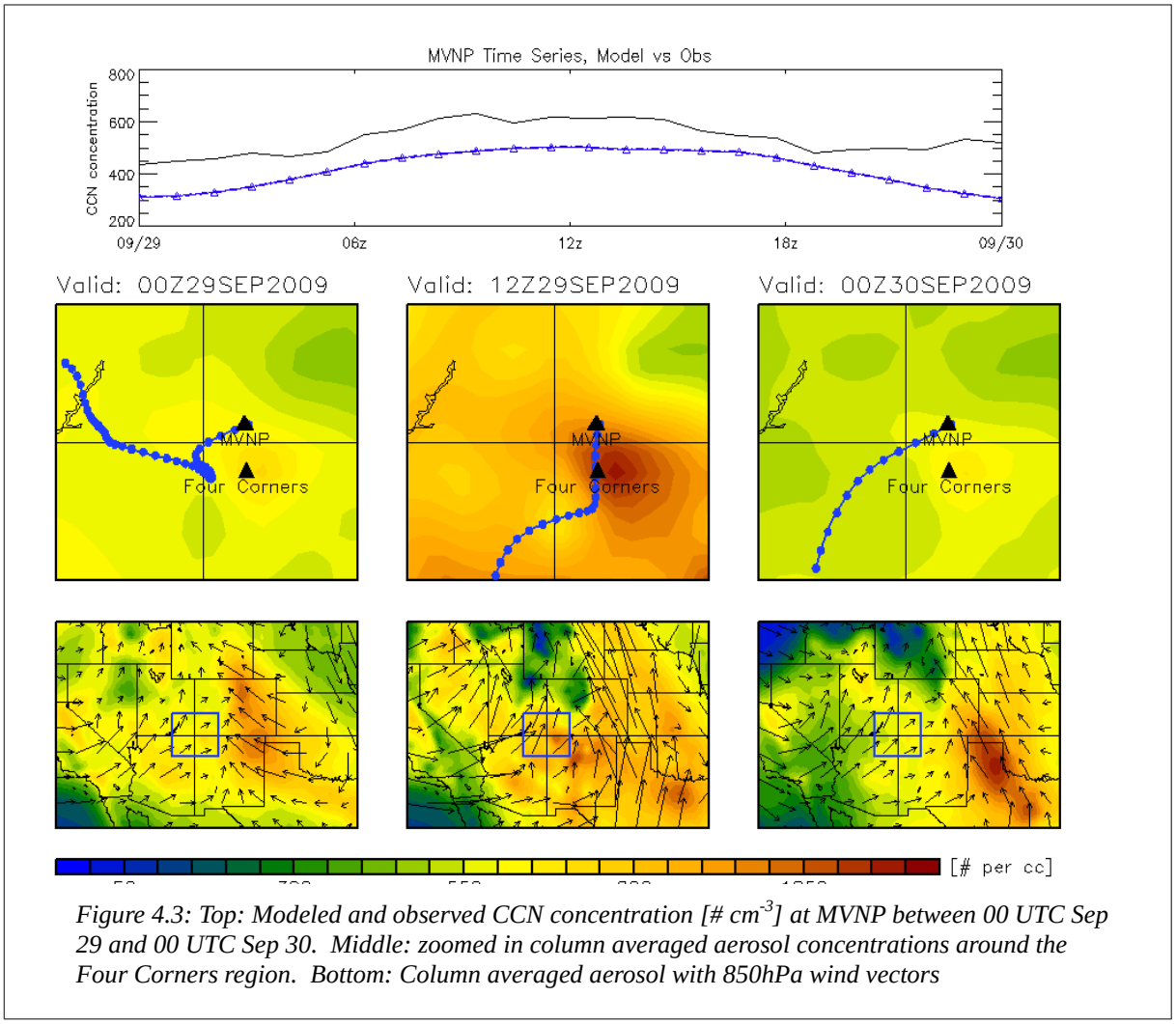

Figure 4.3: Top: Modeled and observed CCN concentration [# cm^{-3}] at MVNP between 00 UTC Sep 29 and 00 UTC Sep 30. Middle: zoomed in column averaged aerosol concentrations around the Four Corners region. Bottom: Column averaged aerosol with 850hPa wind vectors

seen in WRF-CHEM. Because RAMS seems to perform reasonably well, as determined from comparisons to both the ISPA-III observations and to WRF-CHEM, it can be used to diagnose some of the variance observed at MVNP during 09/29 00 UTC and 09/30 00 UTC. Of particular

interest are the relative contributions of local and remote aerosol sources to the total aerosol within the inter-mountain west region.

It was speculated both by Ward et al. (2011), and in Chapter 2 of this thesis that the nearby pollution sources to the southeast play an important role in controlling the observed aerosol concentrations at MVNP, and by extension the Colorado Western Slope. It has also been suggested that remote aerosol sources (particularly ones upwind relative to the mean synoptic flow) have a substantial influence here as well. Fig. 4.3 shows the observed and modeled CCN concentration at MVNP as well as the RAMS near-surface column-averaged aerosol concentration for three time-periods between 09/29 00 UTC and 09/30 00 UTC. Additionally, Fig.4.3 shows a zoomed in view of the Four Corners region, with 850hPa back trajectories plotted from MVNP. This figure shows the influence of remote aerosol sources on CCN concentrations in the Colorado Rockies. At the onset of the aerosol increase at MVNP, it can be seen from the left most panel (00 UTC Sep 29) that the low-level synoptic flow had oriented itself in such a way that air was being advected into the region from the southeast associated with the return flow around a surface high located on the Great Plains, as well as from the southwest associated with the winds ahead of the building trough. It can also be seen from this panel that there are relatively polluted regions both to the southeast and southwest of MVNP. The next panel (12 UTC Sep 29) shows the aerosol field concurrent with the maximum observed CCN concentrations at MVNP. The modeled high concentrations present in the Four Corners region are a result from a buildup of pollution that originated in the urban centers of Los Angeles and Houston. It can also be seen from the bottom center panel that the low-level winds, which were advecting pollution from Texas into the Four Corners region, are no longer doing so, instead they are advecting it north into the Great Plains. The next panel (00 UTC Sep 30) shows the aerosol

fields at the end of the time-period, in which the CCN concentration has dropped by 200 (cm^{-3}) from its maximum value. It can be seen in this panel that the aerosol within the region has returned to a much cleaner state. Westerly winds generally dominate the entire Four Corners region, and the area of high pollution originating in Texas was entirely confined areas well east of MVNP. Based upon this model simulation, the influence of remote aerosol is not trivial. Furthermore, this simulation illustrates the importance of including aerosol sources that are typically *downwind* of the area of study as well as *upwind*.

Examining the importance of local sources apart from remote sources is somewhat difficult as it is hard to isolate one aerosol source from another. The influence of remote sources is easier to diagnose as it is easy to see aerosol traverse the domain with the mean wind. Local sources however are more difficult to view as they will often be enhanced or overshadowed by larger scale aerosol features. The center panels in Fig. 4.3 illustrate this problem. The enhanced aerosol associated with the Four Corners power plant can be easily discerned at all three times, appearing as a local maximum in aerosol field. The back trajectories indicate that air reaching MVNP at the time concurrent with the maximum CCN concentration traverses directly over the Four Corners power plant. The left/right-center panels show back trajectories that do not intersect the Four Corners plant, corresponding with lower CCN concentrations. This lends support to the theory that aerosol from this source affects MVNP. However, the center panel (12 UTC Sep 29) shows high aerosol concentrations covering the entire Four Corners region, associated with the aerosol pollution from remote sources, so the relative role of the local source cannot be easily determined. It is certainly likely that, without remote aerosol sources, the modeled aerosol concentration at MVNP would have shown a similar increase during this time period, but it would have been less of an increase. To investigate the relative role of the local

source to the remote sources, RAMS was run on a much smaller domain centered over MVNP, such that the remote aerosol sources were not included. The model was run for the time-period between 09/28 00 UTC – 09/30 00 UTC, allowing for a 24 hour spin up period. By performing this simulation, the relative influence of local vs. remote aerosol sources can be more quantitatively assessed.

The small domain simulation showed reasonable similarities in the meteorological fields, despite a smaller domain and a finer resolution. The top panel of Fig. 4.4 shows the time-series of aerosol at MVNP for both the small and large domain simulations. This figure illustrates the importance of the remote aerosol sources. Both in the small domain and the large domain simulations there is an increase in aerosol coincident with a period of southerly winds that bring aerosol to MVNP from the Four Corners power plant. This is consistent with the observations. However, the amount of aerosol in the small domain case does not bring nearly as much as the large domain case does, highlighting the importance of remote aerosol sources. The ratio of the small domain aerosol taken over the large domain aerosol indicates that the local aerosol sources amount to roughly 40 to 50% of the total aerosol. It is interesting that during the time at which the wind trajectories were most favorable for transporting aerosol from the Four Corners power plant into MVNP, the relative contribution of local aerosol sources decreased. The fact that remote aerosol sources seem so important to the aerosol burden at MVNP explains the lack of statistical significance in the comparison of aerosol observations at MVNP to wind direction. This model suggests that the pollution advected into MVNP under southeast winds from the Four Corners power plant accounts for less than half of the variance in aerosol concentration, thus this pollution will not show as strong of a signal in the observations. The small domain simulation is not as informative as the large domain simulation, but it does help illustrate the relative

importance of local vs. remote pollution sources in driving atmospheric aerosol concentrations. Additionally, it builds confidence in the RAMS emissions scheme, as it proves that RAMS is able to simulate, to a reasonable degree, a process that has been suggested to play a role in

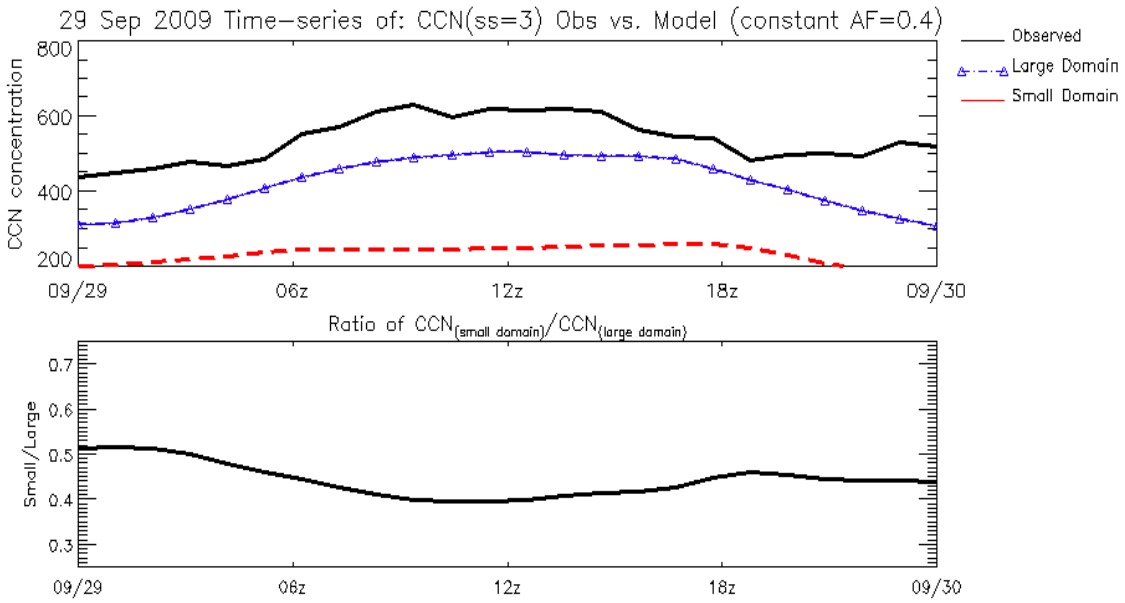

Figure 4.4: Top: Modeled and observed CCN concentration [# cm^{-3}] (00 UTC Sep 29 - 00 UTC Oct 1). Bottom: Ratio of Small/Large domain aerosol concentration.

driving the aerosol concentrations at MVNP.

There is a relatively high degree of confidence that RAMS was able to accurately simulate the transport of aerosol from polluted areas into the more remote region of the Colorado Rockies during this 24 hour period. However, there is still some question regarding how well the model was able to perform for the remainder of the study, particularly during the period associated with orographic precipitation. It is during the analysis of this time period that the differences between the NARR, the NCEP, and the WRF-CHEM simulations become very apparent, and the importance of aerosol scavenging is brought into full perspective.

As it was discussed previously, the RAMS simulation that was initialized and nudged using NARR data was unable to produce significant areas of clouds and precipitation. As a

result, large discrepancies between the NARR and the NCEP simulations appeared in the predicted aerosol fields. . It's interesting that the N ARR simulation, because it lacked precipitation and scavenging, was more comparable to WRF-CHEM. Fig. 4.5 illustrates this by showing the precipitation rates for each simulation and the column average aerosol number concentration at 15 UTC 30 Sept, the time in which the cold front was approaching the Four Corners region. The effect of aerosol scavenging is clearly visible in this figure, as seen by the high aerosol number concentrations associated with areas of precipitation in the NARR and the WRF-CHEM simulations, but not the NCEP simulation.

The comparison between WRF-CHEM and the NARR aerosol fields show surprising similarities, especially during the passage of the trough through the Western US. Both models show a large area of high aerosol concentrations along the trough axis, though WRF-CHEM is more aggressive with respect to aerosol concentrations throughout the whole domain. The most stunning similarity between the two models is the appearance of an appendage of high aerosol concentration that develops on the southwest edge of the trough and moves south through California (this is seen in the bottom left panels of Fig. 4.5). This feature is also faintly visible in the NCEP simulation. The fact that RAMS is able to produce a relatively small scale feature that is also present in WRF-CHEM suggests that the emission scheme performs reasonably well in transporting aerosol throughout the domain. Furthermore, it provides a fair degree of confidence in the location of the aerosol sources used in the RAMS simulations.

The results from this case-study are encouraging. The fact that the emissions parameterization in the RAMS model did much better overall than WRF-CHEM with respect to simulating the aerosol concentrations observed at MVNP, and the fact that the RAMS model was able to simulate some of the same features in the aerosol fields as WRF-CHEM, suggest that this

scheme will prove a reasonable alternative against using WRF-CHEM to predict atmospheric aerosol concentrations. This case-study also helped gain a rough estimate of the relative contributions from local and remote aerosol sources to the total aerosol concentration. Furthermore, these simulations did not require a large amount of computational expense, which speaks to the biggest strength of the emissions scheme presented here. However, the accuracy of this parameterization cannot be wholly determined from one simulation, further validation of this scheme was done by performing a different case-study.

4.3: Case 2: October 12th 2009: 00 UTC – October 15th 00 UTC

4.3.1: Synoptic Overview

Similar to the first case-study discussed, the 12 Oct – 15 Oct 2009 case also involved the passage of a synoptic wave as it moved west-to-east through the domain. This case however, carried a greater amount of moisture, and was a more prolific producer of rain. In fact, it was during this time period that some of the only precipitation recorded during ISPA-III was measured.

The case-study began with the Four Corners region under moderate zonal flow aloft forced by a tightened pressure gradient associated with a trough situated to the north. At the surface, the region was under clear mild conditions with light and variable winds. These conditions persisted until 00 UTC 13 Oct. At this time, the winds aloft were shifting from west to southwest, as a trough was entering the western part of the domain. During the time-period between 00-12 UTC on 13 Oct the surface winds in and around MVNP were generally from the south, though somewhat variable. The weather was still calm, however, to the west,

precipitation was occurring on the California coast and in the Sierra Nevada Mountains ahead of an approaching shortwave trough. As time progressed further the shortwave continued to progress eastward, and became negatively tilted. During this time, scattered showers were able to form in the inter-mountain west, and this corresponded with the time period in which MVNP recorded measurable precipitation. During the time between 12 UTC 13 Oct and 00 UTC 14 Oct, a second system was moving into the Pacific coast, and reinforcing the unsettled weather over California. As this system began to affect the California coast, a weak ridge had built over the Four Corners region as the first system moved east. As time progressed throughout October 14th, the storm affecting California continued to move east, bringing widespread precipitation to the inter-mountain west, including most of Washington, Oregon, Idaho and Nevada. Scattered precipitation also developed in the mountains of Utah and Colorado. At 00 UTC 15 Oct, the storm was starting to occlude and the upper-level trough had propagated north out of the domain, leaving generally zonal flow over the entire western US.

The aerosol observations taken during this time at MVNP were much more complex and varied than they were for the first case-study. This is seen in the time-series of observed aerosol at MVNP between 00 UTC 12 Oct and 00 UTC 15 Oct (Fig. 4.6). From this figure it can be seen that two HPE's occurred during this case-study, which complicates the comparison between the model and the observations. However, there was a period between 12 UTC 13 Oct and 12 UTC 14 Oct where the CCN concentration varied under a constant activated fraction. This period received the most attention in the model comparison analysis.

In general, the first 12 hours of the case-study were characterized as having relatively constant aerosol concentrations, with moderate fluctuations in CCN associated with variations in

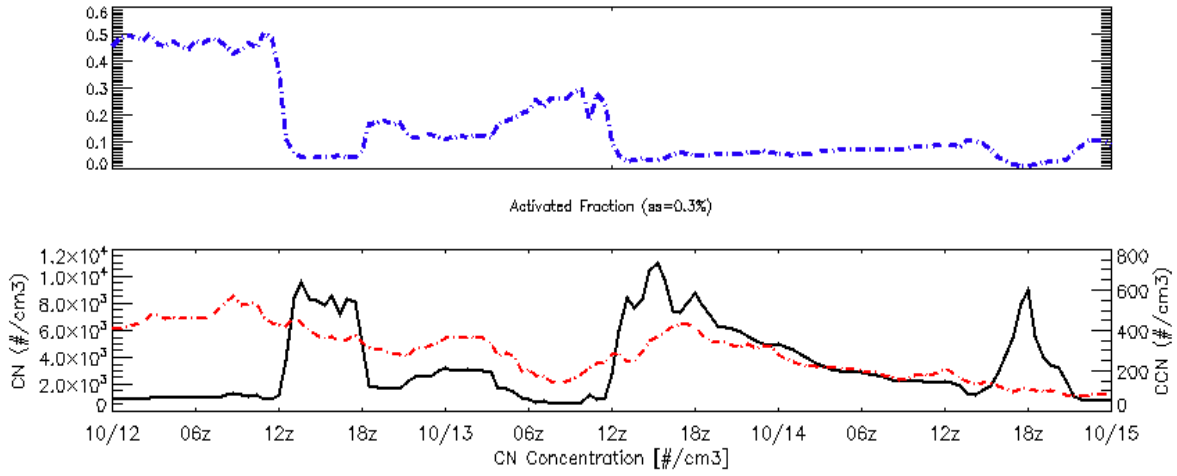

Figure 4.6: Observed aerosol time-series at MVNP: Top: activated fraction. Bottom: CN concentration (Black, scaled by left axis), and CCN (ss=0.3%) (Red, scaled by right axis)

AF. The first HPE occurred between the hours of 12 -18 UTC on 12 Oct. No notable weather was occurring at MVNP during this time. The winds were generally out of the south, and strengthened throughout the time-period. It is possible that as the winds strengthened more numerous smaller particles and high VOC gas concentrations from local sources to the south had made their way into MVNP, before they were able to coagulate into larger aerosol. This would be consistent with the theory presented by Ward et al., but it is still speculation. Between 00-06 UTC 13 Oct, the winds slackened and shifted to a southeasterly direction. This was associated with a slight increase in aerosol and CCN, which was followed by a decrease that coincided with precipitation at the ISPA-III observation site. Shortly after the precipitation, the 2nd HPE

occurred. The aerosol concentration took a relatively long time (~24 hours) to return to average values after this HPE. It is however during this time, that CCN and CN are best correlated, and most likely to be well represented in RAMS. The last 24 hours of the case study (00 UTC 14 Oct – 00 UTC 15 Oct) are characterized as having generally constant, below average, CCN and CN values, with the exception of a very short lived HPE at 18 UTC on the 14th. The aerosol time-series is highly varied during this case-study, which makes it difficult to compare to the

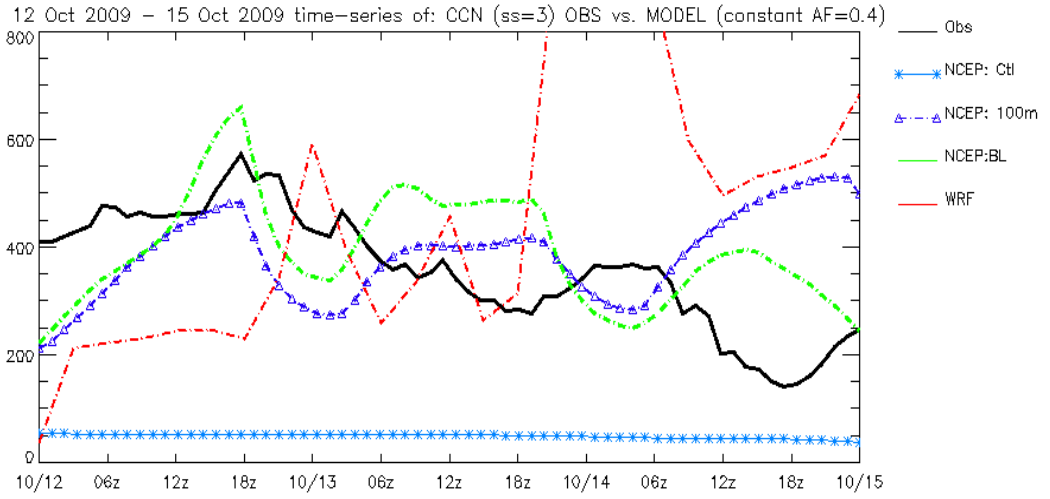

Figure 4.7: Observed CCN compared to the model output CCN [# cm^{-3}] at MVNP for each model simulation

model, but there are time-periods in which a valid model comparison is possible. However, because the aerosol trends observed during this case-study were much more complex than the ones observed during the first case-study, not as much emphasis will be placed on the model comparison.

4.3.2: Model Performance

Both WRF-CHEM and RAMS did a reasonably good job simulating both the synoptic evolution as well as the precipitation associated with this case-study, although there were some

differences in the model with respect to precipitation. The specific differences in precipitation between the two models will not be discussed in detail, but in general RAMS tended to produce more wide spread areas of lighter precipitation than WRF. In the case of both models, the regions of precipitation matched up to the reanalysis data as well as the RADAR and surface observations. Both models did produce precipitation over the MVNP region correspondent with the time that MVNP recorded measurable precipitation. Because both models did well simulating the meteorological aspect of the case-study they can be used to diagnose the aerosol and chemical aspect as well.

4.3.3: Assessment of model performance with respect to aerosol

The time-series of the modeled vs. the observed aerosol concentration is shown in Fig. 4.7. The mean difference between the model and observed aerosol concentration at MVNP is shown in Table 4.3. From Fig. 4.7, it is once again seen that the RAMS parameterization scheme better predicts aerosol concentration than WRF-CHEM. It is seen that the WRF-CHEM aerosol concentration increases rapidly to unrealistic levels with the passage of the main synoptic wave. RAMS does not seem to correlate very well to the observed CCN during this case-study, which may be due to the fact that the observed activated fractions were highly varied. There was a short time-period in which RAMS seemed to correlate reasonably to the observations. This time-period was 18 UTC 12 Oct – 06 UTC 13 Oct. During this time there was a gradual decline in the CCN concentration, which was associated with a constant activated fraction. The model and the observations continue to vary similarly, however 06 UTC marks the beginning of the first HPE, so the comparison between the model and the observations is less meaningful. During the same time-period, WRF-CHEM is anti-correlated with the observations. This is correspondent

with the period of precipitation at MVNP, which suggests the error is related to aerosol scavenging.

Table 4.3: Mean difference between observed CCN and modeled CCN for the 12 Oct 2009 Case

Simulation	Mean	Standard Deviation
Control (CTL)	-316.8	91.78
Z_e=100m (100m)	16.75	118.66
Z_e=BL (BL)	10.71	73.65
WRF	70.69	200.56

The comparison of the aerosol fields between WRF and RAMS at this time, again, show similarities to each other. However, overall WRF-CHEM has more total aerosol than the RAMS model. Fig. 4.8 shows the column-averaged aerosol concentration for WRF-CHEM and RAMS at18 UTC 12 Oct. Both models show an area of enhanced aerosol centered over Nevada with north and eastward extensions into Utah and Wyoming. Both models show generally clean air in far southern California and Arizona. WRF-CHEM shows much higher pollution in New Mexico than RAMS, although RAMS does seem to hint at another pollution maximum that is roughly located in this region. As time progressed, the pollution features moved in the same general direction in both models, although aerosol scavenging in RAMS

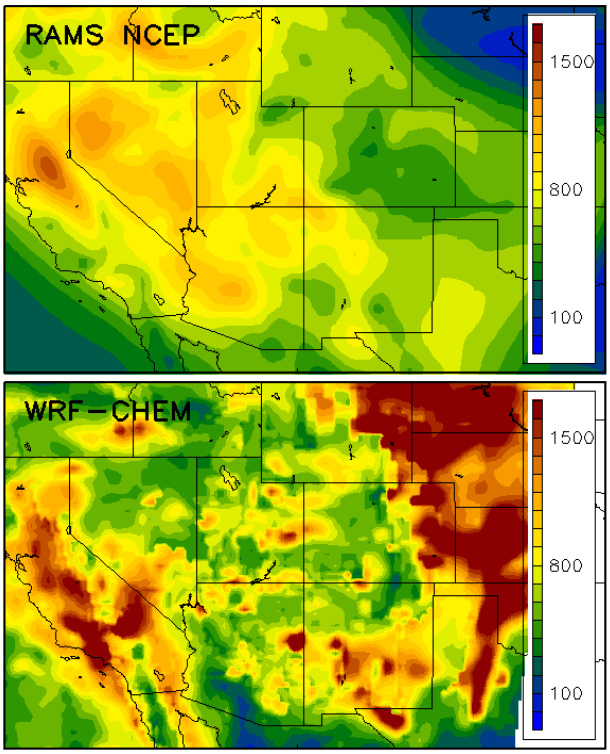

Figure 4.8: Column averaged aerosol concentrations for WRF-CHEM and RAMS at 18 UTC 12 Oct 2009

removes the majority of the pollution in Northeast Nevada and Western Utah. The aerosol concentration in the Four Corners region increased during the afternoon on Oct 12th, in association with the pollution feature to the south, but decreased after that. Once precipitation started to cover a substantial portion of the model domain, aerosol scavenging took over, and as a result, the aerosol fields in WRF-CHEM and RAMS were no longer comparable. They remained this way for the remainder of the case-study. The model time-series once again showed that WRF-CHEM grossly over-predicts the aerosol concentration during cold-frontal passages, similar to the first case-study. It is also seen that the RAMS predicted aerosol compares best to the observed aerosol concentrations when z_e=100m. The RAMS predicted aerosol does not correlate as well to the observations as well as they did during the first case-study. There are several potential reasons for this. One reason is that several HPEs occurred during this case-study. Since the RAMS model does not include SOA as a source for aerosol, this certainly could cause discrepancies between the model and the observations. Secondly, this case-study had a much higher amount of precipitation than did the first case-study. As a result, most of the aerosol in the domain was scavenged. This is seen in the aerosol fields as they evolve throughout the case-study. The precipitation that was observed to fall across the inter-mountain west during this time was scattered in nature, and due to the relatively coarse grid-spacing in RAMS, these showers tended to show up more as uniform precipitation. As a result, it is likely that RAMS "over-scavenged," aerosol within the domain. However, despite these deficiencies, RAMS was able to reasonably simulate aerosol emissions and transport during this case-study.

4.4: Discussion and Conclusions

Overall, these case-studies suggest that the emissions scheme in RAMS is able to

reasonably simulate both the emission and the transport of aerosol. In fact there are time-periods within these case-studies that RAMS is able to correlate very well with the observed aerosol concentrations at MVNP. Furthermore, of all the different simulations performed, the simulations that used the emissions scheme best compared to the MVNP observations. This included both, the control simulation in RAMS, and the WRF-CHEM simulations. This suggests that using RAMS to predict atmospheric aerosol concentrations by initializing aerosol sources using the emissions inventory contained in WRF-CHEM is a more favorable approach than using WRF-CHEM to periodically nudge aerosol concentrations in RAMS. This is a result that was seen in both case-studies, where the aerosol number concentration predicted by WRF-CHEM became excessive during frontal passages, whereas the aerosol concentrations in RAMS stayed near the observed concentrations.

Given that there is some reason to believe that this aerosol scheme is producing somewhat realistic results with respect to the observed aerosol concentrations at MVNP, this scheme will be applied to an orographic snow case within the Colorado Rockies to see how pollution impacts the regional snowfall distribution. The results of this case will be discussed in the next chapter.

Chapter 5: Orographic Snow Case Study

In the chapters beforehand, a computationally efficient aerosol emissions scheme for the RAMS 6.1 model framework was discussed and tested. The results presented in the previous chapter suggest that while this scheme does lack in some regards, it can produce reasonable representations of aerosol with relatively low computational expense. Since the primary objective of this research was to develop this parameterization to support future studies aimed at refining the estimates of the ISPA effect in Colorado, it was deemed important to use this scheme as part of an orographic snow case-study. To keep things as simple as possible, a case study that had been simulated and discussed previously by Saleeby et al., (2008) was chosen for repetition. By repeating a case already presented in the literature, the results of the model simulations can assume a higher degree of confidence. This simulation will serve as the first attempt to quantitatively estimate the anthropogenic influence on orographic snow using a horizontally heterogeneous aerosol field that is representative of nature.

Previous modeling studies have focused mainly on determining the sensitivity of orographic precipitation to CCN by changing, uniformly, CCN concentrations throughout the model domain. The microphysical processes that take place within orographic clouds as a result of changes in CCN concentration are well documented and discussed in the literature review in Chapter 1. Furthermore, a detailed assessment of model performance will not be presented, as this is beyond the scope of this research. Instead, the results presented here will focus primarily on the precipitation differences seen between the emissions scheme and a spatially homogeneous CCN increase. This chapter will address questions that have previously gone unanswered: Are certain areas favored over others for this effect due to closer proximity, or more direct wind trajectories, to pollution sources? These are questions that cannot be addressed by uniformly

increasing CCN concentrations in the model domain. It is hopeful that the results of this chapter will provide a good first assessment of these questions.

5.1: Model set up

The RAMS model was set up for the orographic snow case that occurred in northwestern Colorado from Feb 11th - 12th 2007. This case fell within the measurement period of the ISPA-II field campaign that took place at the Storm Peak Laboratory (SPL) during the winter of 2007. The measurements taken within this case are well described by Saleeby et al. (2008), making this case a good choice for study. Similarly, Saleeby et al. used the RAMS model to simulate this case with varying background CCN concentrations. In doing this, they were able to determine how sensitive this storm was to changes in CCN concentrations. This case was chosen for repetition here, as it had clouds with relatively high LWC, making it highly susceptible to changes in CCN (Saleeby et al. 2008).

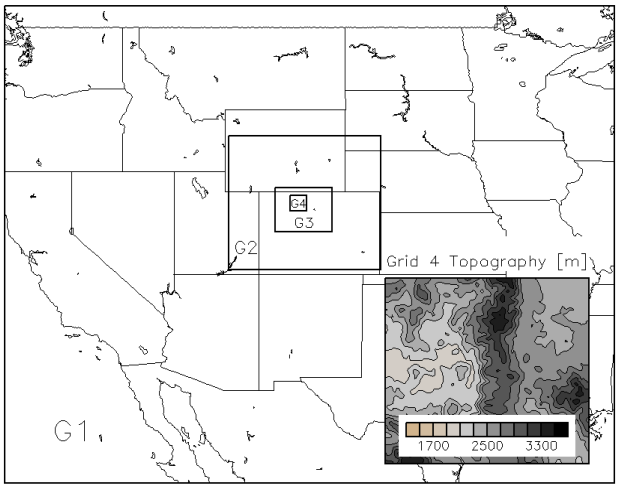

Figure 5.1: Model domains for the nested SPL orographic snow case study

The model parameters used were almost identical to the parameters used by Saleeby et al., with the only major difference being that in this research, the RAMS model was initialized and nudged using the GFS dataset, while Saleeby et al. used the NARR. Additionally, a newer version of RAMS was used in the simulations discussed here. The model was set up with 4 two-way nested grids centered over SPL. A visual representation of this model set up is shown in Fig.5.1, and the model details are presented in Table 5.1. The model was run for three

simulations, a clean control (CLEAN) simulation that used a surface background CCN concentration of 100 (cm^{-3}), a polluted (DIRTY) simulation that used a surface background CCN concentration of 1900 (cm^{-3}), and a simulation that used the emissions scheme (EMISS). In the EMISS simulation, the background CCN was initialized with 100 (cm^{-3}), identical to the CLEAN simulation. For all three simulations, the initial aerosol concentration was given a vertical structure such that the surface aerosol concentration decreased linearly with height until the 4km level, above which the concentration was 100 (cm^{-3}). In all three simulations, aerosol chemistry was represented by κ (initialized as 0.25 for all vertical levels), and the aerosol median diameter was fixed as 40nm. For the EMISS simulation, the pollution mapping was derived from the WRF file described in Chapter 3 (Fig.3.2) and was interpolated to fit all 4 grids. The model was given 24 hours of spin up time before data were analyzed.

In all three model simulations, cloud droplet nucleation was not considered to be an aerosol sink, similar to Saleeby et al. (2008). It was determined that including cloud droplet nucleation as an aerosol sink, without droplet evaporation as a source caused an over-scavenging error within RAMS, which lead to unrealistic precipitation amounts within the model.

Table 5.1: RAMS model set up for the orographic snow case study: Feb 11-13th 2007.

Model Aspect	Setting			
Grid	Grid 1	Grid 2	Grid 3	Grid 4
	62x50	54x50	97x82	114x114
	Δx/Δy=60000(m)	Δx/Δy=15000(m)	Δx/Δy=3000(m)	Δx/Δy=750(m)
Domain Center (Lat, Lon)	40.0, -106.0	40.3, -106.5	40.2, -106.4	40.6, -106.75
Vertical Structure	40 vertical-levels: Δz: stretched from 75m at surface to a maximum of 750m Model-top: 16500m			
Nest type	Two-way			
Initialization and Nudging	1º GFS, nudged every 6hr			
Orography	Reflected envelope			
Radiation	Harrington			
Coarse grid boundary condition	Klemp-Wilhelmson			
Cumulus parameterization	Kain-Fritsch (coarse grids only)			
Microphysics	Binned riming Background CCN Concentration: 100 # cm^{-3} (CLEAN and EMISS) 1900 # cm^{-3} (DIRTY) Background GCCN Concentration: $1x10^{-3}$ # cm^{-3} Background κ: 0.25 CCN median radius: $0.04x10^{-4}$ cm Aerosol Radiative Properties: Off			
CCN Emissions (EMISS Simulation Only)	Constant Rate Emission File: WRF Aerosol File Z_e = 100m Nudge Frequency: 300s			

5.2: Results

The total accumulated precipitation for this case compared well to the total accumulated precipitation from Saleeby et al. (2008). The spatial distribution of total accumulated precipitation in grid 4 is shown for the CLEAN simulation in Fig 5.2. In general, the heaviest amounts of

precipitation were located upwind near the crests of local topographical barriers. The largest area of heavy precipitation occurred near the crest on the north-south oriented Park Range, consistent with the findings from Saleeby et al. The only notable difference between the results of this simulation and the Saleeby et al. results, was that the bull's-eye of precipitation on the Park Range was shifted slightly south. This difference is minor enough that it can be explained by the small differences between the two simulations, e.g., the use of a different dataset for nudging the parent grid. To further ensure the validity of this simulation, the model output time-series of temperature at SPL was compared to the results from Saleeby et al. It was found that the temperature trends were in good agreement with each other. Considering that the results from the control simulation compared reasonably well to the results from Saleeby et al. (2008), it was determined that this model could be used to test the microphysical sensitivity to the emission scheme.

5.2.1: Results for CLEAN vs. DIRTY simulations

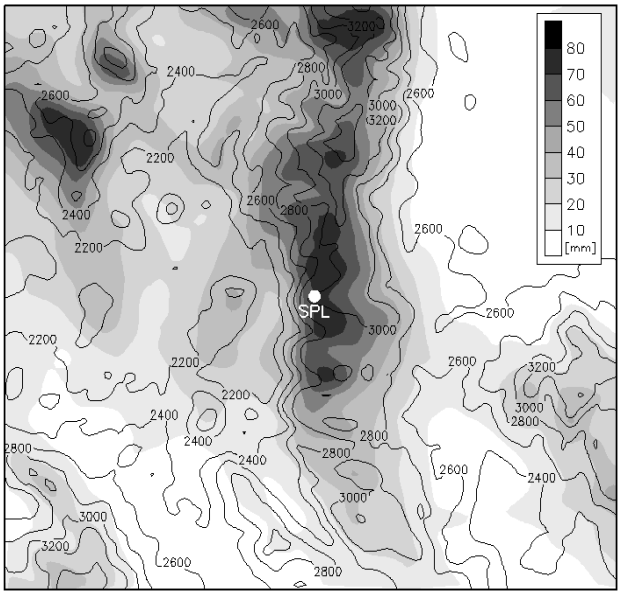

Figure 5.2: Total accumulated precipitation [mm] at the end of the Feb 11 2007 CLEAN simulation

The CLEAN and DIRTY simulations were initialized to be equivalent to the clean and polluted simulations discussed by Saleeby et al. (2008). The plan view in total accumulated precipitation difference between the CLEAN and DIRTY simulations is shown in Fig. 5.3 (a). The ISPA effect is easily discerned

in this figure. The DIRTY simulation generally produced less total precipitation on the upwind sides of local major mountain barriers, and greater amounts of precipitation on the downwind sides, consistent with the spillover effect. This figure shows consistency with the results in Saleeby et al. (2008), although the spatial patterns do not match up exactly. In general the ISPA effect appeared greater, both in magnitude and coverage, for the simulations performed here than it did in Saleeby et al. Also the location of the highest precipitation differences was further south in these simulations. These differences were fairly small, and in general, the overall ISPA effect simulated here was of the same magnitude as the results from Saleeby et al. Furthermore, the domain total precipitation did not show substantial differences in precipitation between the CLEAN and DIRTY simulations, similar to the results from Saleeby et al. (2008). The differences between the CLEAN and DIRTY simulation are adequately discussed in Saleeby et al. (2008), and will not be discussed in more detail here. The DIRTY simulation was performed solely as a means of comparison for the emissions scheme, and not as a means of testing the sensitivity of orographic precipitation to increased CCN.

5.2.2: Results for EMISS simulations

The precipitation differences seen between the CLEAN and the EMISS simulations are of much lower magnitude than the differences seen between the CLEAN and the DIRTY cases (Fig. 5.3 b). This is not surprising as it was thought that the pollution sources used in the EMISS simulation would not lead to aerosol concentrations as high as the concentrations in the DIRTY case. In general however, the same spatial patterns were observed, with a decrease in total precipitation on upwind topographic barriers and an increase downwind. One interesting feature

seen in Fig.5.3 (b) is the presence of a local increase in precipitation in the valley *upwind* of the Park Range. The suspected reason for this is that the inhibition of riming in the EMISS case was sufficient to cause a spillover effect on the small terrain features upwind of the main Park Range barrier. However, once these particles were advected over the small terrain features, they entered a cleaner environment, and were able to collect rime in a relatively unperturbed cloud and precipitate out upwind of the Park Range mountain barrier. This is contrary to the DIRTY case, in which the pollution is uniformly distributed. In this case the particles do not have a chance to rime upwind of the Park Range; instead they are simply advected over this barrier, leading to a more cumulative spillover effect, instead of a more localized one. This is supported by the fact that the large area of increased total precipitation downwind of the Park Range seen in the DIRTY case is not present in the EMISS case. A more detailed view of the differences between the three simulations is seen in an east-to-west cross through SPL (Fig. 5.4). A nearly uniform decrease in accumulated precipitation for the DIRTY case is seen upwind of the Park Range, with an increase downwind, indicative of the spillover effect. The DIRTY case also showed additional localized decreases in total precipitation associated with the smaller topographic barriers upwind of the Park Range, with no corresponding spillover effect. The pre-

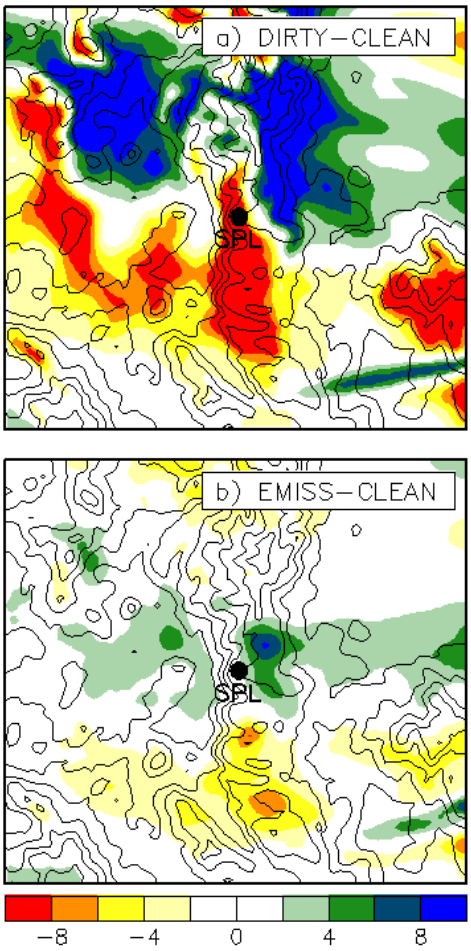

Figure 5.3: Differences in total accumulated precipitation [mm] for the Feb 11 2007 case

cipitation differences between the EMISS and the CLEAN case are much less severe. It can be seen that there were only slight precipitation decreases in the EMISS case upwind of the minor topographic barriers west of the Park Range. It was also seen that the total accumulated precipitation in the EMISS case became equivalent to, or exceeded the total precipitation in the CLEAN case downwind of these features, suggesting a more localized spillover effect. The difference in precipitation between the CLEAN and the EMISS case at the crest of the Park Range is very small. There appears to be a slight spillover effect in this case, but was not nearly as obvious as it was in the DIRTY case. Overall these simulations suggest that the ISPA effect is relatively small, and tends to be more localized, rather than cumulative, in nature. However, because the EMISS simulation included spatially and temporally varying CCN concentrations, it is possible that simulated orographic clouds were subjected to both low and high aerosol concentrations throughout the course of this event. To gather more information regarding the overall spatial pattern seen in the precipitation differences, the time evolution of the aerosol concentrations in grid

4 were investigated. For the duration of the event, the aerosol concentrations simulated in the EMISS case remained within close range of the CLEAN case, generally staying lower than 200 (cm^{-3}). At the beginning of the case, the highest aerosol concentrations were located in the northern half of

the grid west of the Park Range, with a second local maximum centered over the in the valley due west of SPL. This pattern remained persistent throughout the first 12 hours of the case-study. This pollution pattern is consistent with the spatial patterns of precipitation seen in Fig.5.3 (b), as some of the largest upwind decreases in precipitation occurred in the northern part of the domain. Between 12 UTC and 18 UTC on 11 Feb, the region was under very clean conditions, with average aerosol concentrations near to, or less than, the CLEAN case throughout the entire grid 4 domain. The highest CCN concentrations observed during this case occurred near the end of the event after the wind had shifted from west to northwest. During this time-period, the highest aerosol concentrations were located in the central and southern part of the domain, with local amounts >200 (cm^{-3}) near SPL. It was seen that the shift

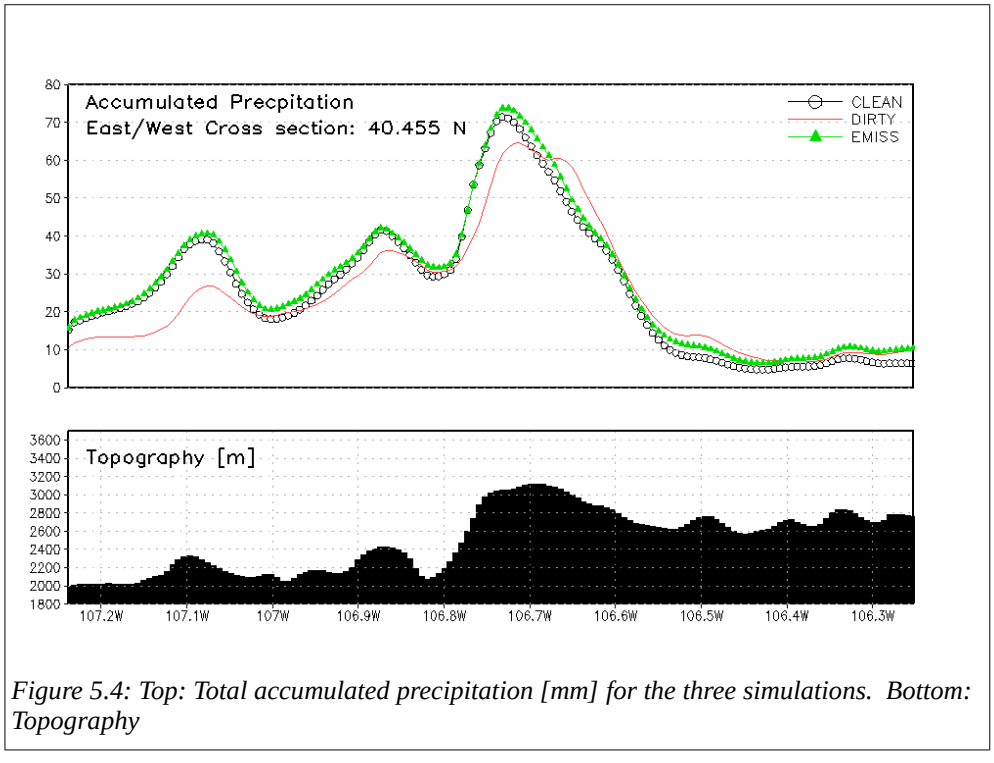

Figure 5.4: Top: Total accumulated precipitation [mm] for the three simulations. Bottom: Topography

from west to northwest winds started advecting more highly polluted air from outside of the grid 4 domain and into the region. To investigate the time-evolution of the ISPA effect, three locations on the crest of the Park Range located within grid 4 were compared (locations shown in Fig.5.5). The time-series average of precipitation rate, Cloud Droplet Number Concentration (CDNC), and Cloud Droplet Diameter (CDD) for each location is shown in Fig.5.6. This figure illustrates the temporal variably in the ISPA effect observed during this case-study. At all three locations, the cloud-droplets are generally smaller (more numerous) in the EMISS case, indicative of a more polluted environment. It was also seen that the differences in DNC and CDD became greater towards the end of the simulation, coincident with the time-period of the highest CCN concentrations. Another interesting feature seen in this figure is a time-period in which there is seemingly no difference in precipitation rate between the CLEAN and EMISS cases. This time-period was coincident with the period of relatively clean aerosol concentrations. Box 2 differed from boxes 1 and 3 in that it was centered over an area in which the total accumulated precipitation was higher for the EMISS case than it was for the CLEAN. From the center panels in Fig.5.6, it is observed that most of the precipitation increase occurred during the beginning of the case, at a time when a local maximum of pollution was in place upwind of this location. It is thought, that the upwind pollution reduced precipitation on the smaller terrain features upwind of the Park

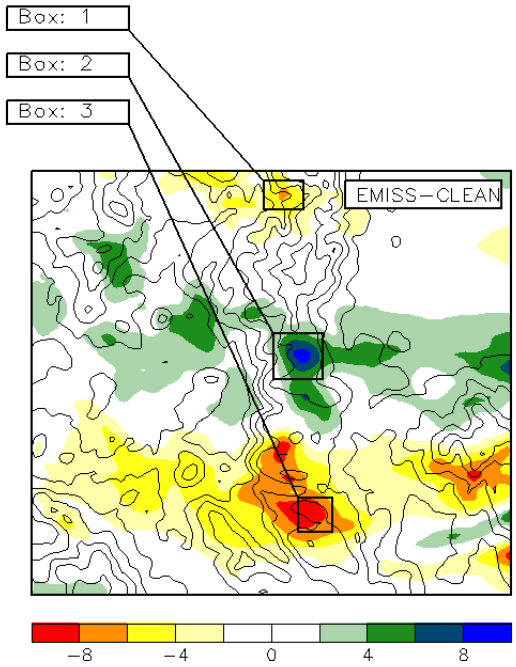

Figure 5.5: Three boxes in which time-averaged of CDNC, CDD, and Precipitation rate were compared. Under laid is the total precipitation differences seen between the EMISS-CLEAN simulations

Range, and allowed more snow-hydrometeors to get advected into a less polluted cloud where they were able to rime and precipitate out, thus increasing the total precipitation. This effect also helps explain the general lack of a significant precipitation decrease along this section of the Park Range seen in the EMISS case. The same analysis shown in Fig.5.6 was performed on the DIRTY case. In general, the decrease in cloud-droplet size was mostly constant (and much greater), and the precipitation rates were uniformly lower throughout the entire case-study at all three locations. It should be noted, that the region encompassed in box 2 showed a decrease in precipitation in the DIRTY case relative to the CLEAN, and not an increase, as was seen in the EMISS case. What this analysis shows is that the real-world ISPA effect is much more complex than the simple sensitivity studies indicate. A good example of this complexity seen as part of this experiment is that cloud-modification from increased CCN has the potential to affect the precipitation rates downstream within relatively unmodified orographic clouds. This result has potentially large implications regarding the real-world ISPA effect, as it indicates a much more complicated response in overall precipitation to pollution than seen in the sensitivity studies.

The increase in pollution seen in grid 4 that occurred in conjunction with a wind-shift indicated the importance of remote pollution sources in this case. Because this was a significant

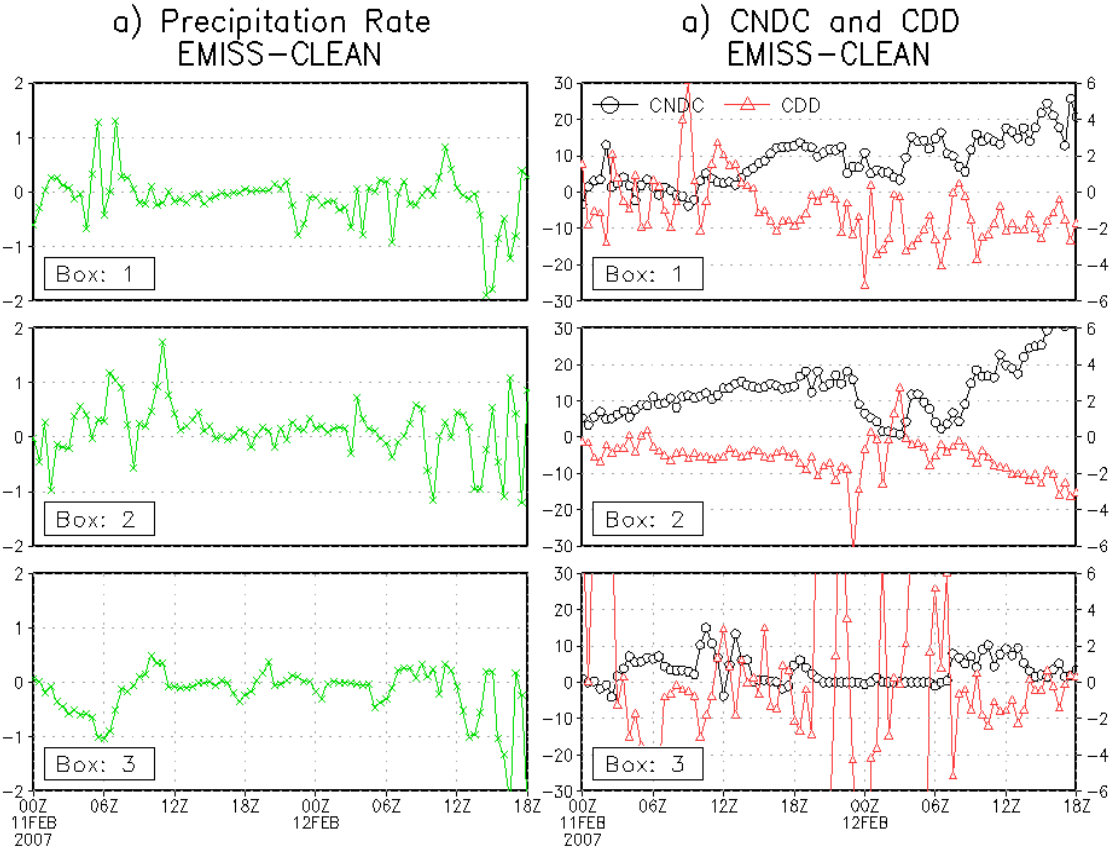

Figure 5.6: Time-series averages for the boxes shown in Fig.5.5. The graphs on the left show precipitation rate in [mm/hr], and the graphs on the right show cloud-droplet diameter (μm) scaled on the right axis, and CDNC (#/cm^{-3}) scaled by the left axis. All graphs are for EMISS-CLEAN.

orographic snowstorm on the Colorado Western slope, with relatively high LWC (Saleeby et al. 2008) it is important to view the transport of aerosol throughout the whole United States to determine how the synoptic patterns in this case advected pollution into the Park Range. At the

beginning of the orographic snow event, a ridge was building into the inter-mountain west region, with generally westerly flow over northern Colorado. West of the region the winds were most southwesterly. Under some circumstances, this would advect polluted air from the Pacific coast towards the Western Slope, however orographic precipitation on the Sierra Nevada mountain range was cleaning the air before it was transported east. As time progressed throughout the storm, westerly flow continued to persist as the ridge started to flatten over the region. At this time, widespread orographic precipitation was occurring in the majority of mountain ranges west of the continental divide, because of this, the air being advected from the west into the SPL region was quite clean. East of the Rockies, near surface aerosol concentrations were quite high as westerly winds across New Mexico and Arizona advected pollution east where it merged with aerosol originating in the urban centers on the Gulf Coast. This plume was then advected north and west with the synoptic wind through the Dakotas and into Montana and Wyoming. As time progressed further, it appears that this pollution was able to wrap around far enough west that it started to influence the Northern Colorado region. Towards the end of the case-study, the Park Range was under generally northwesterly

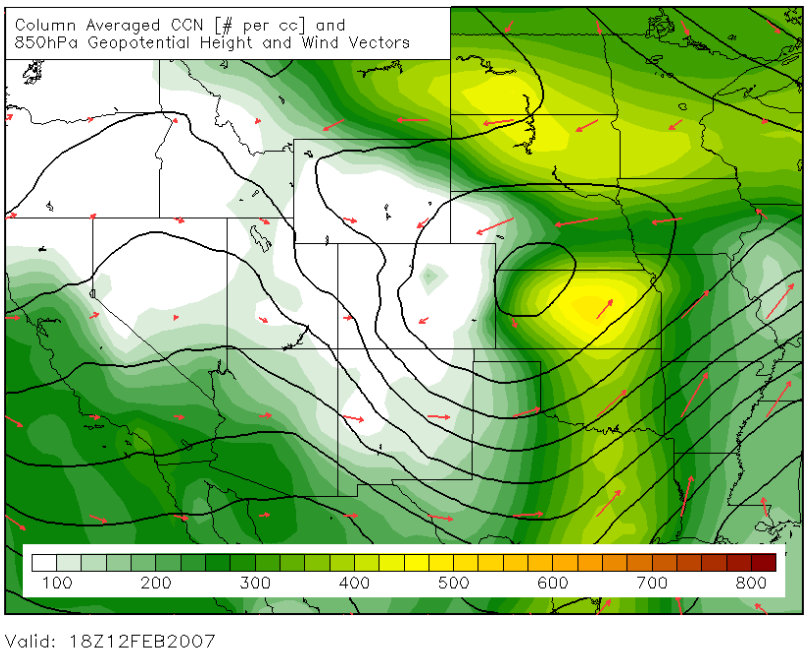

Figure 5.7: Aerosol plume wrapped around the lee-cyclone

flow, which brought south the polluted air, which was further polluted by sources near Rock Springs, WY (Fig.5.7). Similar to the case-studies performed in Chapter 4, this case indicates that typically downwind pollution sources have a potentially large impact on the pollution in the inter-mountain west.

This brief overview of the large scale transport of aerosol during an orographic snow-storm, aids in illustrating the complexity of aerosol pollution, and its real-world effects on pre-cipitation. This is highly evident, in that, this model simulation suggested that CCN originating from Arizona was able to affect Northern Colorado after it had been transported east into the southern Great Plains, then north into the Dakotas, before it was then pulled back west and south through Montana and Wyoming. This is a very circuitous route for the aerosol to take, though it is of potential im-portance in driving the atmospheric CCN con-centration observed at SPL. Furthermore, this simulation suggested that pollution aerosol from the urban centers along the Pacific coast might not play a large role as originally thought, due to the fact

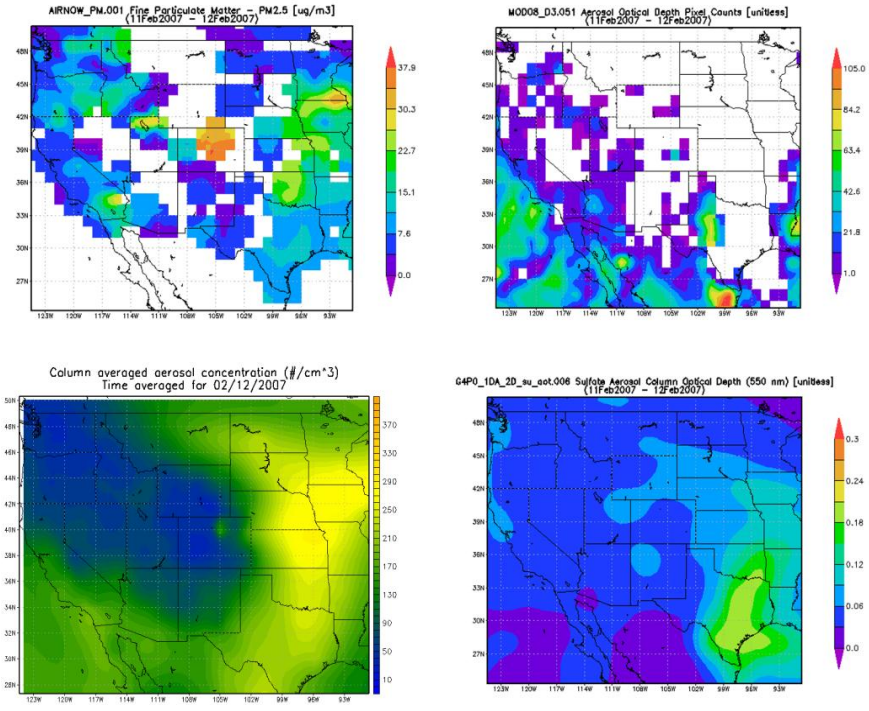

Figure 5.8: Aerosol from RAMS (bottom right), GOCART (Bottom Left), MODIS (Top right) EPA AIRNOW PM2.5 mass (Top Left): Averaged for 12 Feb 2007

that a substantial amount of precipitation occurred upwind of SPL, scavenging a large portion of the CCN before it could be advected to Northern Colorado.

Unfortunately, there is not a large body of observational data available to confirm if the aerosol transport simulated in the model was representative of a real-world feature. Additionally, because WRF Chemistry was not run for this case, an inter-model comparison is not possible. Due to a general lack of comparison data, it is difficult to place a high degree of confidence in the model solution. In fact, the best comparisons available are the relatively coarse (2.5° horizontal resolution) Goddard Chemistry Aerosol Radiation and Transport (GOCART) model, Aerosol Optical Depth (AOD) retrievals from MODIS, and EPA surface PM2.5 measurements. A brief comparison between RAMS, GOCART, PM2.5 and MODIS, while not quantitatively relevant, does seem to show agreement with respect to the placement of a large swath of pollution extending south to north across the Great Plains (Fig. 5.8). This provides a little more confidence in the model, but the observational data required to make firm quantitative comparisons is nonexistent. However, this comparison provides marginal confidence in the RAMS aerosol predicted aerosol fields.

Overall the model simulations discussed here have provided some new insight into the ISPA effect. The control simulation compared very well to the results from Saleeby et al. (2008), providing confidence in the model's ability to perform well in this case. The precipitation differences seen between the EMISS and the CLEAN case revealed that the ISPA effect is much less than previous sensitivity studies have suggested. Furthermore, new complexities regarding the impact of CCN on orographic clouds were seen when using a spatially and temporally varying aerosol field. This is best seen as precipitation particles that fell through polluted clouds were advected over small terrain features west of the Park Range mountain barrier before

entering a relatively clean orographic cloud where they were able to rime and precipitate out. Essentially, the ISPA effect on small terrain features aided in supplying more precipitation particles for the orographic seeder cloud on the main topographic barrier.

This experiment also showed how aerosol pollution can change under different advective regimes. This was seen towards the end of the case-study when higher aerosol concentrations were brought into the domain under northwesterly winds. Coincident with the period of relatively high aerosol concentrations, was an across the board increase (decrease) in CDNC (CDD) at several locations near the crest of the Park Range. Furthermore, this experiment was able to show the importance of remote aerosol pollution to orographic snow on the western slope.

It was seen from the parent grid that an aerosol plume centered over the Great Plains was advected north, and then wrapped west around a lee-cyclone. The increase in aerosol seen in grid 4 was occurring at the same time that the wrap around pollution was being advected into the region, suggesting that the wrap around pollution may have played a role in this case. This result, once again, illustrates the importance of including traditionally downwind aerosol sources in these simulations. Overall this experiment was a success; the emissions scheme performed reasonably well, and the comparison between the CLEAN, DIRTY and EMISS simulations provided new insight regarding the ISPA effect. Most importantly, this experiment serves as a good proof of concept for future simulations using this scheme.

Chapter 6: Discussions and Conclusions

The emissions scheme introduced and discussed throughout this thesis has proven to be a reasonably good representation of the real-world emission and transport of pollution in RAMS.

Certainly, this scheme represents an improvement over previous schemes, both in accuracy and in computational expense. Despite these benefits, some of the assumptions embedded within the scheme, made to maintain computational efficiency, compromise (to a potentially significant degree) the schemes accuracy. It is important to discuss these assumptions, and potential future improvements, as well as the future goals and research potential associated with the use of this scheme.

The most beneficial aspect of the emissions scheme presented here is, by far, the low computational expense. The low computational expense of this scheme makes it possible to simulate entire winter seasons at fine spatial resolution over the Colorado western slope with a representation of pollution. However, the reduction in computational expense came at a price; the complex chemical processes involved in aerosol formation and growth had to be simplified.

The largest deficiencies of this parameterization are that; it is assumed that a large part of SA can be represented as primary aerosol, and aerosol size is treated as a constant. A third deficiency, although less important than the other two, for these short term simulations, was that emission rates were held constant in time. The first two assumptions are critical for maintaining a low computational expense, but substantially reduce the real-world representativeness of the model with respect to CCN prediction. The ability for an aerosol to serve as a cloud condensation nucleus is dependent entirely on its size and chemical makeup. Therefore, eliminating one of these dependencies as a variable certainly affects the aerosol activation ratios within the model. Of these two dependencies, the ability for an aerosol to activate as a cloud nucleus is most dependent on aerosol size (Dusek et al. 2006). This implies that the constant size assumption will essentially fix the activation ratio within the model to a constant, with a relatively small variations associated with minor changes in κ. By recalling the observational

data from MVNP discussed in chapter 2, a constant activation ratio is not a realistic representation of the real world. However, the constant size assumption greatly simplified this scheme and ensured model stability with respect to the aerosol properties.

Aerosol size is dependent on the total aerosol mass, the aerosol number concentration, and the density of the aerosol particles. The RAMS model uses aerosol number concentration and a fixed aerosol median diameter corresponding to a fixed size distribution to calculate a total aerosol mass (assuming a fixed density). In the scheme presented here, aerosol number concentration is the prognosticated variable, and mass is calculated as a function of the number concentration and the fixed median diameter. In order to predict aerosol size properly within the model, aerosol mass would have to be included as a prognostic variable as well as number concentration. A simple treatment of aerosol size as a passive tracer within the model will not suffice, as the size would not be properly represented in regions of divergence. Furthermore, because aerosol size is explicitly related to the condensation of gas-phase chemicals, it cannot be represented as a source dependent variable. It is because an appropriate representation of aerosol size requires mass to be prognostic instead of calculated, and because aerosol mass cannot be represented well as a source dependent variable that aerosol size was assumed constant in this scheme. Furthermore, assuming size to be constant makes the computation of κ simple, and reduces the overall computational expense.

As mentioned in the first chapter of this thesis, SA is a large contributor to the total aerosol burden. As such, it is important to clarify the justification behind the decision to represent SA as primary aerosol in this emissions scheme. Similar to the constant size assumption, the main reason for neglecting explicit SA formation processes is the reduction in computational expense. The development of a reasonable SA formation scheme requires the

generation, depletion, and interaction of several new three-dimensional scalar arrays, as well as their interaction with aerosol. This parameterization would further complicate the calculations of aerosol mass, size, concentration, and κ. The decision to neglect SA formation within this parameterization was not taken lightly, and a lot of work was put into justifying this decision. After an extensive literature review, and comprehensive analysis on data from both ISPA-III and IMPROVE, it was determined that, during the winter months, SA formation does not make up a large contribution of the total aerosol burden. The relative minimum in SA during the winter is primarily due to the decrease in organic VOC's originating from vegetation, though diminished photochemical activity also plays a role (Liao et al. 2007 and Schichtel et al. 2008***)***. In addition to decreased SA formation during the winter, it was found that most of the anthropogenic SA generally forms on short timescales near urban centers (Volkamer et al. 2006***)***, and can therefore be treated as primary aerosol. For these reasons, it was determined that the emissions scheme would reasonably represent number concentrations that reflected the contributions of SA, particularly near urban centers and point sources, as primary aerosol, without including the chemical processes involved in SA formation.

The third deficiency worth discussing is the assumption that the emissions rate at all locations is held constant in time. In the real-world the amount of pollution added to the atmosphere (especially in urban areas) is strongly related to time-of-day and season (Mayer, 1999). In addition to regular diurnal and seasonal cycles in aerosol mass concentration, weekly cycles in aerosol concentration have also been measured (e.g., Murphy et al. 2008 and Mayer, 1999). The reason for the observed diurnal cycle is relatively straightforward, in addition to the fact that there is more anthropogenic pollution during the daylight hours (more vehicular traffic) photochemical reactions are actively oxidizing VOC gases and SO_2, contributing to the

production of secondary aerosols, and in the growth of existing aerosols. Similarly to the diurnal cycle, the seasonal cycle is also associated with photochemical activity. The observed weekly cycle in aerosol concentration is thought to be entirely anthropogenically forced and associated primarily with automobile emissions (Xia et al. 2008). Considering there are several known temporal cycles in both aerosol concentration anthropogenic emissions the treatment of emission rate as constant in time is a potentially significant deficiency in the model. For shorter numerical simulations, neglecting the seasonal and weekly cycles is likely not a bad assumption. However, the diurnal cycle poses more of a problem, as the diurnal variation in emission rate is not trivial (Zhang et al. 2004). While, it is likely that this deficiency is not as important as the constant size assumption, or the lack of SA formation processes, it is certainly worth mentioning in the discussion.

While these deficiencies are relevant as part of this discussion, it is important to view them within the context of this research. Aerosol number concentration (within the accumulation mode) is the most important variable in determining the number of active CCN within a cloud, with aerosol size and chemistry having only a secondary influence. This suggests that the constant aerosol size assumption is not a large deficiency, so long as the model is able to predict aerosol concentration with reasonable accuracy, which this parameterization has proven capable of doing. As part of its validation, this scheme was used in case-study simulations using RAMS. The aerosol fields from these simulations were then compared to the WRF-CHEM aerosol fields for the same case-studies. The results of this validation showed that the RAMS emission scheme compared reasonably well to the WRF-CHEM model, signifying this schemes ability to capture aerosol emissions in a reasonable way. In fact, the largest differences between the two models occurred near frontal boundaries and over areas of precipitation. These differences can be

largely attributed to microphysical differences between the two models, specifically aerosol scavenging. Additional validation of this scheme revealed that it was able to reasonably predict the time-evolution of the observed CCN concentration at MVNP. Given that this parameterization is able to predict aerosol concentrations reasonably well, the deficiencies associated with the scheme's simplifying assumptions do not grossly diminish the confidence in its ability to predict CCN. Because this scheme has proven to be a worthwhile means of introducing aerosol emissions and chemistry in RAMS, it is worth discussing some improvements that could potentially increase both the accuracy, and the utility of it.

6.1: Future Improvements of the Model Scheme

This parameterization serves as a great start in the implementation of an easy to use, reasonably accurate aerosol emission scheme into RAMS. However, there is room for future improvement. This section serves as an opportunity to discuss some potential improvements for this parameterization, specifically in regards to some of the assumptions made previously.

Perhaps the simplest improvement is the introduction of a diurnally variable aerosol emission rate. While the daytime increase in aerosol concentrations over urban areas is mostly driven by SA formation processes, much of the research on air quality indicates that the diurnal variability in urban pollution follows a simply sinusoidal curve (e.g., Mayers 1999, Zhang et al., 2004). Introducing such a relationship where the base emission rate is adjusted by a factor proportional to the sine of local time (or TOA incoming solar radiation), would be relatively easy to implement, and would not significantly increase the computational expense. Introducing this parameterization would likely have a measurable effect on simulations that are geared towards phenomenon on relatively short timescales, e.g., convection, but it is unknown as to whether or not this parameterization would affect the results of simulations that span a much longer time. A

potentially more significant improvement to the scheme would be to remove the constant aerosol size assumption.

Because the ability for aerosol to serve as CCN is highly dependent on aerosol size, this could be highly beneficial for future simulations. However, by allowing aerosol size to vary requires that aerosol mass be a prognostic variable as well as number. This brings more complexity into the model. Additionally, new limits on aerosol size would need to be imposed in the model to ensure that the aerosol median radius stayed within the bounds of the nucleation look-up-tables. These new requirements and extra calculations would cause non-trivial increases in computational expense. At current, due to a general lack of information regarding aerosol size, including it as a variable in RAMS simply does not appear worth the added computational expense. Furthermore, aerosol size is less variable during the winter months in remote continental areas due to reduced SOA formation (Levin et al. 2011), so there is not much benefit in trying to parameterize it in this scheme.

The lack of SA formation processes within this parameterization is perhaps its biggest limitation. While this research has made a strong case for the acceptance of this assumption, particularly in regards to wintertime simulations, the lack of SA places limits on the utility of this parameterization. This problem is a much trickier one to tackle than the constant radius size problem. This is because it is very difficult to develop a worthwhile SA parameterization short of developing a full chemistry resolving model, defeating the overall purpose of saving computational resources. In the future, as further advancements are made in computer power, and in the WRF-CHEM model, perhaps returning to an approach similar to the one used by Ward et al. (2011) is warranted.

6.2: Final Conclusions

Throughout the course of this chapter, much of the discussion has been focused on pointing out the flaws in the parameterization developed as part of this research. While these flaws are not trivial, and while they certainly limit the confidence in this scheme, it should be reiterated that, despite these flaws, this scheme was able to do a reasonable job predicting aerosol concentrations. In addition to producing reasonably accurate CCN concentrations, this scheme also proved capable of predicting κ to a reasonable extent. While κ ultimately does not have as great an effect on the CDNC within a cloud as does the actual aerosol concentration, the inclusion of an accurate representation of κ in this scheme provides a first step in representing aerosol composition and chemistry in RAMS.

In both ISPA-III case-studies, the RAMS model was able to more accurately predict the aerosol concentration at MVNP than WRF-CHEM, with the most significant improvement being that it eliminated the high-bias associated with wet scavenging intrinsic to the WRF-CHEM aerosol modules. Second, this method was able to perform reasonably well with a very low computational expense relative to the Ward et al. (2011) method. This is the most attractive aspect of this scheme. Considering that aerosol concentration is the most important variable in determining the CDNC, the fact that this scheme performs fairly well with respect to CCN concentration far outweighs it's poor representation of activated fraction associated with the constant-size assumption. In addition to proving a reasonably good way to predict aerosol concentrations, the simulations using scheme provided some insight regarding the behavior of aerosol pollution.

Because this parameterization does not include a representation of SA formation, some interesting conclusions could be easily drawn regarding the sources of origination for aerosol in

the inter-mountain west. Most notably were the contributions of pollution sources well *east* of the Rocky Mountains to the total aerosol burden west on Colorado Western Slope. At the beginning of this research it was thought that the majority of the pollution that plays a role in affecting snowstorms in the Rocky Mountains originated from the major urban centers west of the region. In fact, based on this research, a significant portion of this pollution may originate from sources well east. This was shown in both the ISPA-III case-studies, where aerosol originating from Houston and other cities along the Texas coast was advected into the Four Corners region under easterly flow around an area of high pressure, and the in SPL orographic snow case, where polluted air east of the Front Range was wrapped around a lee-cyclone and pulled back south along the Western Slope. These results suggest that in order to accurately simulate the CCN impacts on water resources in Colorado, the model domain needs to include sources well east of the region, as well as sources to the west.

To conclude, the aerosol emissions scheme presented as part of this thesis provides a simple and efficient way to tie atmospheric CCN concentrations to real-world pollution. This scheme substantially improves upon the previous method which required case and time-dependent three-dimensional WRF-CHEM output by both, significantly reducing the computational expense, and by removing errors associated with aerosol scavenging. Additionally, this model proved capable of use in a high resolution nested simulation of an orographic snow case study, providing new insight regarding the overall effect pollution has on wintertime precipitation in the Colorado Rockies. We hope that the emissions scheme described here will be used in future modeling studies to help better understand the impact on CCN clouds and precipitation.

6.3: Future Work

This parameterization has proven to be useful, and we hope that it can be used for a wide range of future modeling studies. More specifically, this scheme will be most useful in further refining estimates of the impact of pollution (as CCN) on water resources within the inter-mountain west. This is because this entire parameterization was built with this goal in mind. The logical next step in this study would be to use this parameterization to repeat the season-long simulations performed by Saleeby and Cotton (2011).

A second potential study related to the ISPA effect, would be to use this parameterization as part of a case study that includes dust. As discussed in Chapter 2, dust makes up the majority of total aerosol mass in the region encompassing the Colorado western slope during the spring. Therefore dust likely has a large influence on orographic precipitation during the spring. Unfortunately time-constraints did not allow for such a simulation to be performed as part of this research, so it is included as a recommendation for future work.

Lastly, because this scheme is both easy to use and flexible, it is possible that its utility goes far beyond that of orographic snow simulations. For example, it could be used to simulate the interaction of convection with urban centers (similar to Carrio and Cotton, [2008]).

References:

Albrecht, B. A., 1989: Aerosols, cloud microphysics, and fractional cloudiness. *Sci*,m **245**,1227-1230.

Andrea, M.O., and D. Rosenfeld, 2008: Aerosol-cloud-precipitation interactions. Part 1. The nature and sources of cloud-active aerosols. *Earth. Sci. Rev.*, **89**, doi:10.1016/j.earscirev.2008.03.001.

Borys, R.D., D.H. Lowenthal, S.A. Cohn, and W.O.J. Brown, 2003: Mountaintop and radar measurments of anthropogenic aerosol effects on snow growth and snowfall rate. *Geophys. Res. Lett.*, **30**, doi:10.1029/2002GL016855.

Borys, R.D., D.H. Lowenthal, and D.L. Mitchell, 2000: The relationships among cloud microphysics, chemistry, and precipitation rate in cold mountain clouds. *Atmos. Env.*, **34**, 2593-2602.

Borys, R.D., and M. Wetzel, 1997: Storm Peak Laboratory: A reseach, teaching, and service facility for the atmospheric sciences. *Bull. Amer. Meteo. Soc.*,**78**, 2115-2123.

Cozic, J., B. Verheggen, E. Weingartner, J. Crosier, K. N. Bower, M. Flynn, H. Coe, S. Henning, M. Steinbacher, S. Henne, M, Collaud Coen, A. Petzold, and U. Baltensperger, 2008: Chemical composition of free tropospheric aerosol for PM1 and coarse mode at the high alpine site Jungfraujoch. *Atmos. Chem. Phys.*, **8**, 407-423.

Cruz, C. N., and S. N. Pandis, 1997: A study of the ability of pure secondary organic aerosol to act as cloud condensation nuclei. *Atmos. Env.*, **31**, 2205-2214.

Delene, D. J., and T. Deshler, 2001: Vertical profiles of cloud condensation nuclei above Wyoming. *J. Geophys. Res.*, **106**, 12,579-12,588

Dusek, U., G. P. Frank, L. Hildebrandt, J. Curtius, J. Schneider, S. Walter, D. Chand, F. Drewnick, S. Hings, D. Jung, S. Borrmann, and M. O. Andreae, 2006:Size Matters More Than Chemistry for Cloud Nucleating Ability of Aerosol Particles. *Science*, **312**, DOI: 10.1126/science.1125261.

Givati, A., and D. Rosenfeld, 2004: Quantifying precipitation suppression due to air pollution. *J. App. Met.*, **43**, 1038-1056.

Guenther, A., T. Karl, P. Harley, C. Wiedinmyer, P. I. Palmer and C. Geron, 2006: Estimatesof global terrestrial isoprene emissions using MEGAN (Model of Emissions of Gases and Aerosols from Nature). *Atmos. Chem. Phys., **6**, 3181-3210.*

Heymsfield, A.J., and R.M. Sabin, 1989: Cirrus crystal nucleation by homogeneous freezing of solution droplets. *J. Atmos. Sci*, **46**, 2252-2264.

Hoyle, C. R., M. Boy, N. M. Donahue, J. L. Fry, M. Glasius, A. Guenther, A. G. Hallar, K. Huff Hartz, M. D. Petters, T. Petäjä, T. Rosenoern, and A. P. Sullivan, 2011: A review of the antrhopogenic influence on biogenic secondary organic aerosol. *Atmos. Chem. Phys.*, **11**, 321-343.

Intergovernmental Panel on Climate Change (IPCC), 2007: Climate Change 2007: Synthesis report, Geneva, 104pp.

Kanakidou, M., J. H. Seinfeld, S. N. Pandis3, I. Barnes, F. J. Dentener, M. C. Facchini, R. Van Dingenen, B. Ervens, A. Nenes, C. J. Nielsen, E. Swietlicki, J. P. Putaud, Y. Balkanski, S. Fuzzi, J. Horth, G. K. Moortgat, R. Winterhalter, C. E. L. Myhre, K. Tsigaridis, E. Vignati, E. G. Stephanou, and J.Wilson, 2005: Organic aerosol and global climate modelling: a review. *Atmos. Chem. Phys.*, **5**, 1053-1123.

Korolev, A. V., Mazin, I. P., 2003: Supersaturation of Water Vapor in Clouds. *J. Atmos. Sci.*, **60**,2957-2974

Kulmala, M., A. Laaksonen, and L. Pirjola, 1998: Parameterizations for sulfuric acid/water nucleation rates. *J. Geophys. Res.*, **103**, 8301-8307.

Liao, H., D.K. Henze, J.H. Seinfeld, S. Wu, and L.J. Mickley, 2007: Biogenic secondary organic aerosol over the United States: Comparison of climatological simulations with observations. *J. Geophys. Res.*, **112**, doi:10.1029/2006JD007813.

Levin, Z., and W. R., Cotton, 2009: Aerosol pollution impact on precipitation, Springer, 386pp.

Levin, E. J. T., A. J. Prenni, M. D. Petters, S. M. Kreidenweis, R. C. Sullivan, S. A. Atwood, J. Ortega, P. J. DeMott, and J. N. Smith, 2012: An annual cycle of size-resolved aerosol hygroscopicity at a forested site in Colorado. *J. Geophys. Res.*,**117**,doi:10.1029/2011Jd016854.

Levin, E. J. T., S. M. Kreidenweis, G. R. McMeeking, C. M. Carrico, J. L. Colleg, Jr., and W. C. Malm, 2009: Aerosol physical, chemical and optical properties during the Rocky Mountain Airborne Nitrogen and Sulfer study. *Atmos. Env.*, **43**, 1932-1939.

Lohmann, U., 2003: Can anthropogenic aerosols decrease the snowfall rate? *J. Atmos. Sci.*, **61**, 2457-2468.

Lowenthal, D. H., R. D. Borys, W. R. Cotton, S. M. Saleeby, S. A. Cohn, and W. O. J. Brown, 2011: The altitude of snow growth by riming and vapor deposition in mixed-phase orographic clouds. *Atmos. Env.*, **45**, 519-522.

Lynn, B., A. Khain, D. Rosenfeld, and W. L. Woodley, 2007: Effects of precipitation from orographic clouds. *J. Geophys. Res.*, **112**, doi:10.1029/2006JD007537.

Mayer, H., 1999: Air Pollution in Cities. *Atmos. Enviroment*, **33**, 4029-4037.

McKeen, S., S. H. Chung, J. Wilczak, G. Grell, I. Djalalova, S. Peckham, W. Gong, V. Bouchet,

R. Moffet, Y. Tang, G. R. Carmichael, R. Mathur, and S. Yu, 2007: Evaluation of PM2.5 forecast models using data collected during the ICARTT/NEAQS 2004 field study. *J. Geophys. Red.*, **112**, D10s20, doi:10.1029/2006JD007608.

Muhlbauer, A., T. Hashino, L. Xue, A. Teller, U. Lohmann, R. M. Rasmussen, I. Geresdi5, and Z. Pan, 2010: Intercomparison of aerosol-cloud-precipitation interactions in stratiform orographic mixed-phase clouds. *Atmos. Chem. Phys. Discuss.*, **10**, 10487–10550.

Murphy D.M., Capps S.L., Daniel J.S., Frost G.J., White W.H., 2008: Weekly patterns of aerosol in the United States. *Atmos Chem. Phys.*, **8**, 2729–2739

Petters, M.D., and S. M. Kreidenweis, 2007: A single parameter representation of hygroscopic growth and cloud condensation nucleus activity. *Atmos. Chem. Phys.*, **7**, 1962-1971.

Petters, M.D., and S. M. Kreidenweis, 2007: A single parameter representation of hygroscopic growth and cloud condensation nucleus activity – Part 2: Including Solubility. *Atmos. Chem. Phys.*,**8**, 6273-6279.

Pringle, K.J., H. Tost, A. Pozzer, U. Pöschl, and J. Lelieveld, 2010: Global distribution of the effect aerosol hygroscopicity parameter for CCN activation. *Atmos. Chem. Phys.*, **10**, 6301-6339

Raga, G. B., and P. R. Jonas, 1994: Vertical distribution of aerosol particles and CCN in clear air around the British isles. *Atmos. Env.*,**29**, 673-684

Rauber, R.M., 1981: Microphysical processes in two stably stratified orographic cloud systems. M.S. thesis, Dept. of Atmospheric Science, Colorado State Univeristy Atmospheric Science Paper 337 151 pp.

Saleeby, Stephen M., William R. Cotton, 2008: A Binned Approach to Cloud-Droplet Riming Implemented in a Bulk Microphysics Model. *J. Appl. Meteor. Climatol.*, **47**, 694–703. doi: http://dx.doi.org/10.1175/2007JAMC1664.1

Saleeby, S.M., and W.R. Cotton, 2004: A large-droplet mode and prognostic number concentration of
cloud droplets in the Colorado State Regional Atmospheric Modeling System (RAMS). Part I: Module descriptions and supercell test simulations. *J. Appl. Meteor.*, **43**, 1912-1929.

Saleeby, S.M., W.R. Cotton, D. Lowenthal, R.D. Borys, and M.A. Wetzel, 2008: Influence of Cloud Condensation Nuclei on Orographic Snowfall. *J. Appl. Meteorol. Clim.*, **48**, doi:10.1175/2008JAMC1989.1.

Saleeby, S.M., W.R. Cotton, and J.D. Fuller., 2011: The cumulative impact of cloud droplet nucleating aerosols on orographic snowfall in Colorado. *J. App. Meteo.* **50**, 604-625.

Schichtel, B. A., W. C. Malm, G. Bench, et al. (2008), Fossil and contemporary fine particulate

carbon fractions at 12 rural and urban sites in the United States, J. *Geophys. Res.-Atmos*., **113**.

Sørenson, J.H., A. Rasmussen, 1996: Forecast of atmospheric boundary layer height utilised for ETEX real-time dispersion modelling. *Phys. Chem. of Earth.*, **21**, 435-439.

Strader, R., F. Lurmann, S.N. Pandis, 1999: Evaluation of secondary organic aerosol formation in winter. *Atmos. Env.*, **33**, 4849-4863.

Twomey, S., 1974: Pollution and the Planetary Albedo. *Atmos. Env.*, **8**, 1251-1256.

U.S. Environmental Protection Agency, 2009: 2005 National Emissions Inventory Data and Documentation, http://www.epa.gov/ttnchie1/net/2005inventory.html.

Volkamer, R., J. L. Jimenez, F. San Martini, K. Dzepina, Q. Zhang, D. Salcedo, L. T. Molina, D. R. Worsnop, and M. J. Molina, 2006: Secondary organic aerosol formation from anthropogenic air pollution: Rapid and higher than expected. *Geophys. Res.*, **33**, doi: 10.1029/2006GL026899.

Ward, D. and W. R. Cotton, 2011: A method for forecasting CCN using predictions of aerosol physical and chemical properties from WRF/Chem. *J. App. Met. Clim.*, **50**, 1601-1615.

Ward, D. S. and W. R. Cotton, 2010: Cold and transition season cloud condensation nuclei measurments in western Colorado. *Atmos. Chem. Phys.*, **11**, doi:10.5194/acp-11-4303-2011.

Xia, X., T. F. Eck, B. N. Holben, G. Phillippe, and H. Chen ,2008,, Analysis of the weekly cycle of aerosol optical depth using AERONET and MODIS data, *J. Geophys. Res*., **113**, D14217, doi:10.1029/2007JD009604.

Xue, L. A. Teller, R. Rasmussen, I. Geresdi, Z. Pan, and X. Lui, 2012: Effects of aerosol solubility and regeneration on mixed-phase orographic clouds and precipitation. *J. Atmos. Sci.*, doi:10.1175.JAS-D-11-098.1, in press.

Yu, Shaocai, 1999: Role of Organic acids (formic, acetic, pyruvic and oxalic) in the formation of cloud condensation nuclei (CCN): a review. *Atmos. Res.*, **53**, 185-217.

Zhang, R., Wenfang Lei, Xuexi Tie, and Peter Hess, 2004:Industrial emissions cause extreme urban ozone diurnal variability. *PNAS*, **101**, doi: 10.1073/pnas.0401484101.

NORTH AMERICAN REGIONAL REANALYSIS (NARR): A long-term, consistent, high-resolution climate dataset for the North American domain, as a major improvement upon the earlier global reanalysis datasets in both resolution and accuracy, Fedor Mesinger et. al, submitted to BAMS 2004.

Appendix 1: Locations of IMPROVE stations used in this study

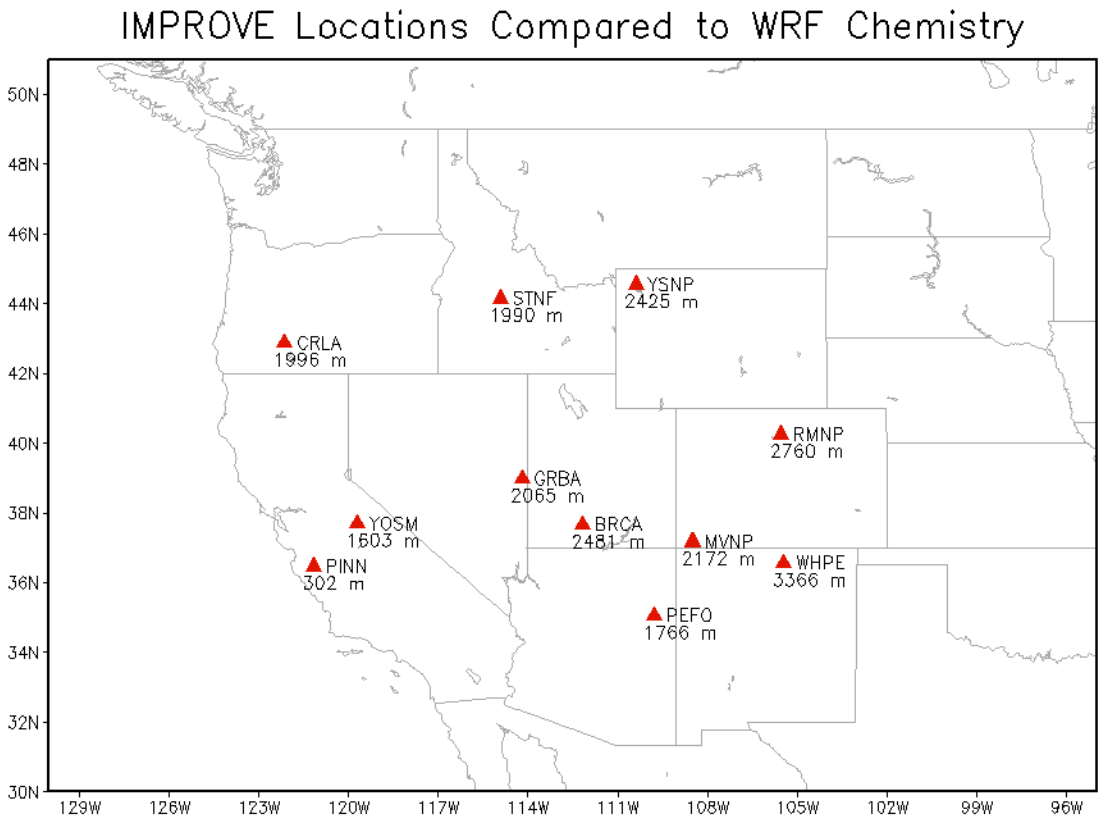

1. BRCA: Bryce Canyon National Park
2. CRLA: Crater Lake National Park
3. GRBA: Great Basin National Park
4. MVNP: Mesa Verde National Park
5. PEFO: Petrified Forest National Park
6. PINN: Pinnacles National Monument
7. RMNP: Rocky Mountain National Park
8. STNF: Sawtooth National Forest
9. WHPE: Wheeler Peak
10. YOSM: Yosemite National Park
11. YSNP: Yellowstone National Park